Acta Biomaterialia 9 (2013) 5855–5875

Contents lists available at SciVerse ScienceDirect

Acta Biomaterialia

journal homepage: www.elsevier.com/locate/actabiomat

Review

Sintering of calcium phosphate bioceramics

E. Champion *

Université de Limoges, CNRS, SPCTS UMR 7315, Centre Européen de la Céramique, 12 rue Atlantis, 87068 Limoges Cedex, France

ARTICLE INFO

Article history:
Received 27 July 2012
Received in revised form 22 November 2012
Accepted 26 November 2012
Available online 2 December 2012

Keywords:
Review
Sintering
Calcium phosphates
Bioceramics
Bone graft substitutes

ABSTRACT

Calcium phosphate ceramics have become of prime importance for biological applications in the field of bone tissue engineering. This paper reviews the sintering behaviour of these bioceramics. Conventional pressureless sintering of hydroxyapatite, $Ca_{10}(PO_4)_6(OH)_2$, a reference compound, has been extensively studied. Its physico-chemistry is detailed. It can be seen as a competition between two thermally activated phenomena that proceed by solid-state diffusion of matter: densification and grain growth. Usually, the objective is to promote the first and prevent the second. Literature data are analysed from sintering maps (i.e. grain growth vs. densification). Sintering trajectories of hydroxyapatite produced by conventional pressureless sintering and non-conventional techniques, including two-step sintering, liquid phase sintering, hot pressing, hot isostatic pressing, ultrahigh pressure, microwave and spark plasma sintering, are presented. Whatever the sintering technique may be, grain growth occurs mainly during the last step of sintering, when the relative bulk density reaches 95% of the maximum value. Though often considered very advantageous, most assisted sintering techniques do not appear very superior to conventional pressureless sintering. Sintering of tricalcium phosphate or biphasic calcium phosphates is also discussed. The chemical composition of calcium phosphate influences the behaviour. Similarly, ionic substitutions in hydroxyapatite or in tricalcium phosphate create lattice defects that modify the sintering rate. Depending on their nature, they can either accelerate or slow down the sintering rate. The thermal stability of compounds at the sintering temperature must also be taken into account. Controlled atmospheres may be required to prevent thermal decomposition, and flash sintering techniques, which allow consolidation at low temperature, can be helpful.

1. Introduction

Several ceramic materials have been commonly used in the medical field for more than 40 years to repair diseased or damaged hard tissue [1]. From the beginning of the 1970s, a first generation of ceramics, called bioinert ceramics, made of alumina, have been successfully implanted. At the same time, increasing interest has been devoted to calcium phosphate materials because of a chemical composition resembling that of bone mineral. Thus, calcium phosphate ceramics (CPC) with expected superior biological properties began to be investigated. CPC belong to the second generation of biomaterials. They have been used in surgery from the 1980s [2–4]. They are called bioactive ceramics, a family that includes mainly calcium phosphate hydroxyapatite $Ca_{10}(PO_4)_6(OH)_2$(HA), tricalcium phosphate $Ca_3(PO_4)_2$(TCP) and biphasic calcium phosphates (BCP, a mixture of HA and TCP). Attempts to increase the biological response and osseointegration of these bioceramics have recently led to investigation of various chemical compositions, architectures and microstructures. Consequently, the processes used to tailor implants have been widely studied. Generally speaking, ceramic processes consist of three main successive steps: powder synthesis, shaping and sintering [5]. This last step consists of high-temperature thermal treatment of a porous powder compact, but at a temperature lower than the melting point. It leads to the final ceramic part by elimination of pores contained in the shaped body. During this treatment, several phenomena induce consolidation and densification of the shaped part. At the same time, particle size and shape may change in a wide range. Reactions may also occur and change the chemical composition and/or the phase composition of the fired product. Therefore, the sintering is of prime importance, because the final properties of the ceramic parts strongly depend on it.

As mentioned by De Groot [4], early use of calcium phosphate powder (TCP) in hard-tissue surgery was published in 1920 [6]. But sintering of hydroxyapatite powder compact in order to produce ceramic parts for medical applications was first reported in the literature only in 1970 by Monroe et al. [7]. A synthetic powder that had a Ca/P molar ratio of 1.54 was die pressed and further sintered at 1300 °C for 15 h, resulting in a dense polycrystalline ceramic made of partially dehydrated HA and α-TCP. Because of the similarities of this ceramic with the mineral composition of bone and teeth, this first prospective study demonstrated the possible

* Tel.: +33 555 87 50 23 63; fax: +33 555 87 50 23 04.
E-mail address: eric.champion@unilim.fr

1742-7061/$ - see front matter © 2012 Acta Materialia Inc. Published by Elsevier Ltd. All rights reserved.
http://dx.doi.org/10.1016/j.actbio.2012.11.029

fabrication of CPC of interest for further dental or orthopaedic prosthetics. From this date, numerous papers investigating CPC of various chemical compositions as well as the use of different sintering methods have been published. They aimed to produce dense or porous parts or particles, coatings and, more recently, nanomaterials or three-dimensional (3-D) scaffolds for bone tissue engineering. A great number of these studies investigated the mechanical properties of sintered CPC. Indeed, low mechanical reliability (strength, toughness) has always been and is still a critical limitation for the use of CPC in hard-tissue prosthetics. The influence of porosity and composition of CPC on the mechanical properties has been reviewed recently [8], and the dependence on grain size for dense materials can be deduced from several works [9–15]. A lot of emphasis is now being placed on nanomaterials or nanostructured materials, which brings specific difficulties because of the nanometric size of particles and their growth during high-temperature heat treatment. Sintering is fundamental, since it provides the final microstructural design (grain size and shape, porosity ratio, pore size) and chemical composition (of grains and grain boundaries) of CPC that directly governs the mechanical performance as well as the biological behaviour. Many papers describe the sintering of CPC, but few have investigated the sintering behaviour itself, i.e. analysis of physico-chemistry and mechanisms. The sintering ability of a ceramic compound depends on various experimental, chemical or physical parameters. Only physico-chemical parameters that are specific to CaP will be detailed hereafter.

This review of the literature is presented showing more elaborate sintering procedures. The range of microstructural features that can be offered by sintering is addressed. The cited references, extracted from the Thomson Reuters Web of Knowledge[SM], were selected for their relevance and interest to the topic. First, this paper focuses on general features of the sintering behaviour of stoichiometric hydroxyapatite. Then, it presents:

(i) the influence of chemical composition on the sintering of CPC, based on the behaviour of HA and TCP; the effect of ionic substitutions or sintering aids and the influence of sintering parameters (atmosphere, time, temperature) are addressed
(ii) the methods used to sinter these CPC; starting with conventional sintering, several other techniques including two-step sintering (TSS), hot pressing (HP), hot isostatic pressing (HIP), microwave sintering (MWS) and spark plasma sintering (SPS) are discussed.

2. Sintering of HA

Sintering of a ceramic powder compact requires accordance with thermodynamic and kinetic conditions [16]. Its fundamentals and physico-chemistry have been widely described in the literature. The following points are summarized from the books of Rahaman (latest edition) [17] and of Bernache-Assollant and co-authors (French edition) [18].

Sintering will occur only when the driving force is sufficiently high. It is possible if the total Gibbs free energy (G) of the system is minimized ($dG < 0$) by decreasing the solid–gas surface area A_{sg} ($dA_{sg} < 0$) of high energy (γ_{sg}), which is replaced by a solid–solid surface area A_{ss} ($dA_{ss} > 0$) of lower energy (γ_{ss}):

$$dG = dA_{ss}\gamma_{ss} + dA_{sg}\gamma_{sg} \quad (1)$$

The driving force of sintering relates to the decrease in surface and interfacial energies of the system by matter transport (atoms or ions), which can proceed by solid, liquid or gaseous phase diffusion. Diffusion is thermally activated, and the limiting species responsible for the effective pathway depends on numerous parameters: chemical and physical properties of the material, and composition of the gaseous atmosphere. Solid-state diffusion during pressureless sintering in air, i.e. "conventional" sintering, is generally involved in the consolidation or densification of CPC. Its physico-chemical features were studied mainly in the case of HA. To a much lesser extent, the use of additives to promote liquid phase sintering or other assisted sintering techniques was also investigated.

2.1. Solid-state pressureless sintering of HA

As pointed out by Landi et al. [19], a first difficulty encountered in the literature concerning the sintering behaviour of HA is the definition of which material is called "hydroxyapatite". Because the sintering behaviour is strongly affected by the chemical composition, some available data refer ambiguously to HA. This is particularly the case when calcium-deficient hydroxyapatite powders (CaDHA) of general formula $Ca_{10-x}(PO_4)_{6-x}(HPO_4)_x(OH)_{2-x}$, with $0 \leqslant x \leqslant 2$, are used. Such compounds are characterized by a calcium-to-phosphorus molar ratio Ca/P < 1.667, and they decompose into BCP above 700 °C [20]. They should not be considered as HA ceramics. In some studies, the term hydroxyapatite is even used when the sintered ceramic contains only TCP [21]. When reactions occur during sintering, the resulting ceramic should not refer to the initial precursor, but to the final compound. Moreover, the apatite structure may incorporate various ions in each one of its crystalline sites. So, only the stoichiometric chemical formula $Ca_{10}(PO_4)_6(OH)_2$, i.e. Ca/P = 1.667, should be considered as HA. This constitutes the first difficulty in the analysis of literature data because, as will be highlighted, information on the chemistry of studied CaP is often missing or incomplete.

At the macroscopic scale, the sintering ability is usually characterized by thermomechanical analysis (TMA, or dilatometry). High-temperature microscopy can also be used for a direct, i.e.in situ, characterization.

Fig. 1 gives a characteristic plot of linear shrinkage vs. the temperature for a compacted sample of stoichiometric HA powder (Ca/P = 1.667). Its derivative curve is given in Fig. 2. Physical

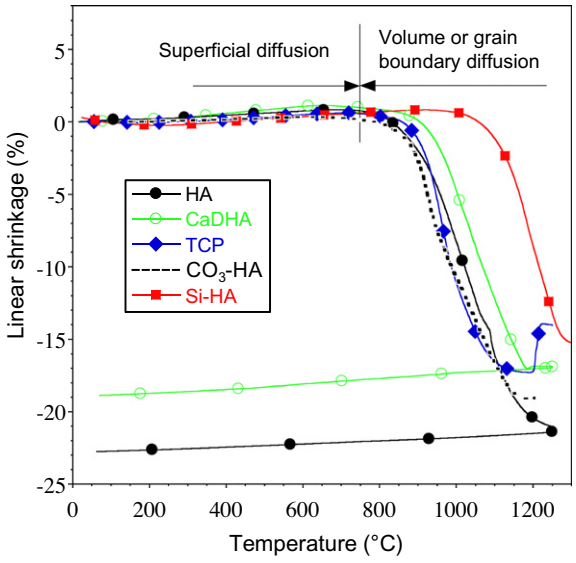

Fig. 1. Thermomechanical analysis. Linear shrinkage of calcium phosphate compacts vs. the temperature in ambient air for HA (Ca/P = 1.667), CaDHA (Ca/P = 1.535), TCP (Ca/P = 1.50), Si-HA (x_{Si} = 0.5 mol) and in CO_2 atmosphere for B-type CO_3-HA (x_{CO3} = 0.95 mol), data from Refs. [22,23,57,145] (specific surface area of initial powders = 30 $m^2\ g^{-1}$).

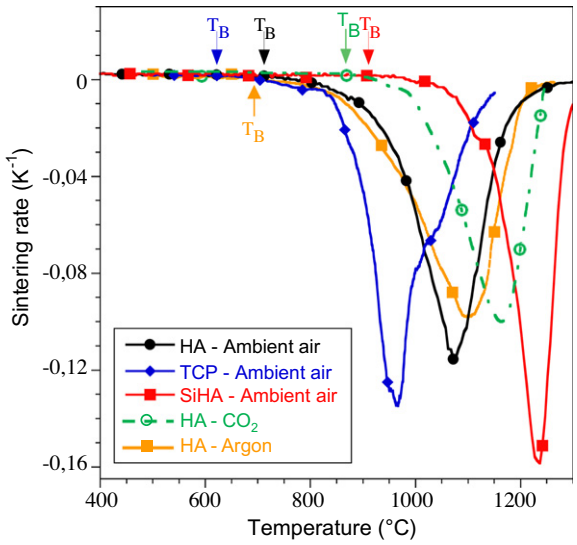

Fig. 2. Derivative plot of TMA for some CaP, data from Refs. [22,23,57,145] (specific surface area of initial powders = 30 $m^2 g^{-1}$).

parameters, such as powder grain size distribution, specific surface area of powder or compacity of shaped body, may change sintering ability and kinetics. They are common to all ceramic systems [17], and their influence will not be detailed hereafter. The data plotted in Figs. 1 and 2 were registered using the same experimental procedure with CaP powders having a similar surface area (30 $m^2 g^{-1}$), which makes comparisons possible.

In the first step, up to ~750 °C, intrinsic expansion of the powder compact occurs. Then, at higher temperatures, densification begins and proceeds by elimination of pores contained in the initial powder compact. The sample shrinks to reach its maximal bulk density.

The sintering of a powder compact is generally divided in three sequential stages [17,18].

(i) In the initial stage the interparticle neck forms and grows. This stage can occur with a light or without densification, and it lasts up to a relative density of ~65% of the "theoretical" (i.e. the value of fully dense material). A simple model of spherical particles [17,18] can be used to schematize the initial powder compact and the changes that occur at the microscopic scale during this stage (Fig. 3a and b).

(ii) In the intermediate stage, densification is generally assumed to occur by the shrinking of the pores. Pores remain open and constitute a continuous phase. This stage covers the major part of sintering, and it ends when the pores pinch off to become isolated, which corresponds to an increase in relative density to ~90%. It is characterized by two temperatures that can be deduced from derivative plots of TMA curves (Fig. 2): T_B, temperature at which the shrinkage begins; T_M, temperature at which the sintering rate is maximum. The main values of T_B and T_M for HA are ~750 °C and 1050 °C, respectively [19,22–24].

(iii) In the final stage of sintering (from a relative density of ~90%), the isolated pores may disappear altogether, leaving a fully or nearly fully dense ceramic.

Then, during cooling to room temperature, the sample retracts in accordance with the expansion coefficient of the sintered ceramic. As shown hereafter, pressureless sintering of HA is generally performed in the temperature range 1100–1250 °C. In this domain, densification occurs without formation of any liquid phase. Structural investigations have confirmed that no secondary phases, either crystalline or amorphous, are formed [25]. Indeed, HA remains stable up to ~1350–1450 °C in ambient air [26–28], the temperature depending on the partial pressure of water vapour [28]. Only partial dehydration of HA into oxyhydroxyapatite may occur [27–30] according to a reversible reaction:

$$Ca_{10}(PO_4)_6(OH)_2 \leftrightarrow Ca_{10}(PO_4)_6(OH)_{2-2y}O_y + yH_2O_{(gas)} \quad \text{(Reaction1)}$$

At the microscopic scale, solid-state diffusion in crystalline solids, which is responsible for sintering, requires the presence of point defects within the crystal structure, and matter motion may proceed through several different diffusion pathways involving superficial, volume or grain boundary diffusion. Superficial diffusion is a mechanism that induces consolidation of a powder compact without densification, while volume or grain boundary diffusion is associated with densification.

2.1.1. First stage of sintering: superficial diffusion

At low temperatures, from ~400 °C, the surface area of HA powder compacts begins to decrease (Fig. 4a) [22,31–33]. The grains weld through the formation of strong chemical bonds, resulting in the appearance of necks between grains (Fig. 3a). These phenomena occur without densification up to ~700–800 °C, as illustrated in Fig. 1. They correspond to the first stage of sintering, leading to the consolidation of the initial powder compact through superficial diffusion. The rate of isothermal surface decrease due to superficial diffusion in CaP apatites of general formula $Ca_{10-x}(PO_4)_{6-x}(HPO_4)_x(OH)_{2-x}$, with $2 \geqslant x \geqslant 0$, was analysed and quantified as follows [22,33]:

$$v = dS/dt = k(T, Ca/P) \times (P_{H_2O})^{0.68} \times S^8 \quad (2)$$

where S is the surface area, P_{H_2O} is the partial pressure of water vapour, and k is a function of the temperature and CaDHA composition.

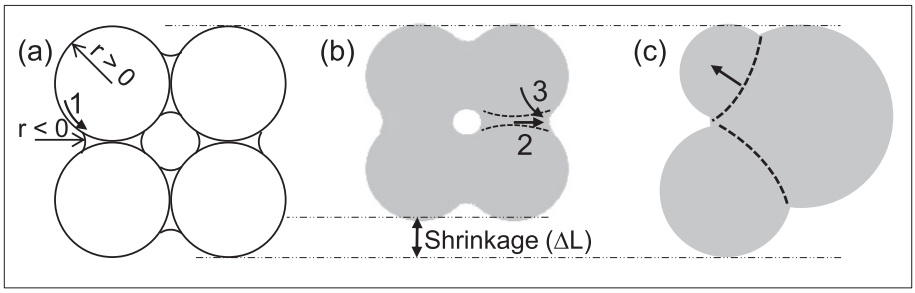

Fig. 3. (a) Adjacent spheres model: consolidation by superficial diffusion (1) and formation of necks between grains. (b) Secant spheres model: consolidation and densification by volume (2) or grain boundary (3) diffusion. (c) Coalescence and grain growth by grain boundary sliding.

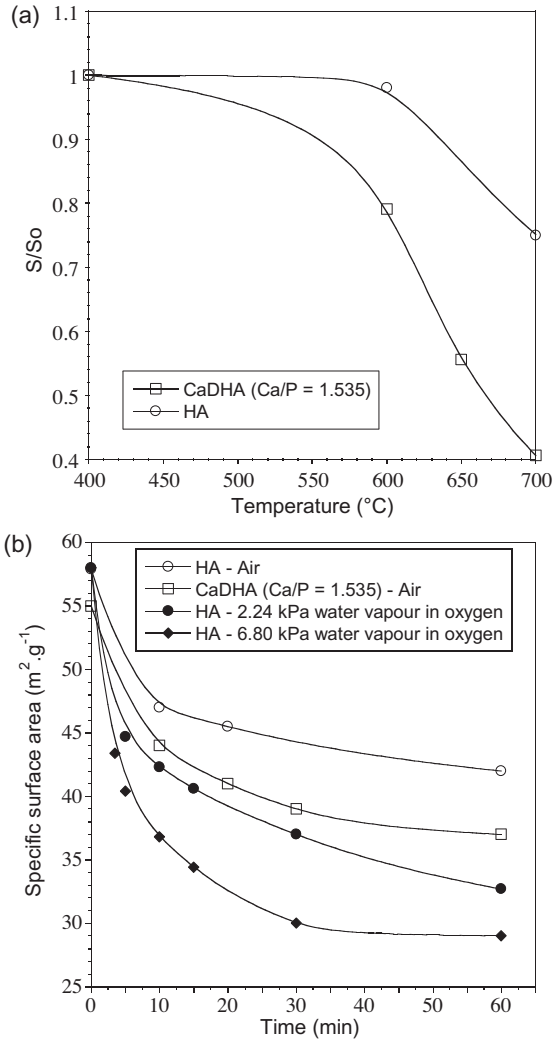

Fig. 4. (a) Normalized surface reduction of HA [31] and CaDHA [22] in ambient air vs.temperature. (b) Surface reduction at 600 °C of HA powder in various atmospheres and CaDHA powder in ambient air, data from Refs. [22,33].

Thus, water vapour in the sintering atmosphere catalyses surface reduction of HA at low temperatures (Fig. 4b). Influence of moisture on the thermal behaviour of some other ceramic oxides was also reported [34]. The temperature dependence of k is due to the thermal activation of superficial diffusion. Depending on the experimental procedures of determination, values for activation energy of superficial diffusion were estimated to be 120 kJ mol^{-1} [33] or in the range 190–290 kJ mol^{-1} [35]. For stoichiometric HA, the rate of surface area reduction remains low, the value of the rate constant k at 700 °C being only 9.2×10^{-3} vs. 1.35 for Ca/P = 1.535 (i.e. $x = 0.79$ in the chemical formula of CaDHA) [22]. In this last case, superficial diffusion at low temperatures is high and leads to important grain coalescence before densification begins. The number of grains decreases, and their size increases by grain boundary sliding (Figs. 3, 5a and b). These results relate to the concentration of calcium and hydroxide vacancies in the HA lattice, which increases with decreasing Ca/P ratio, thus facilitating matter motion. The total solid–gas interfacial energy is drastically reduced ($dA_{sg}\gamma_{sg}$; Eq. (1)). Consequently, the driving force for further sintering at higher temperatures drops. The densification process slows down (Fig. 1; Ca/P = 1.535) and the final microstructures are made of coarse grains with irregular shape (Fig. 5c). The lower sinterability of apatite on decreasing the Ca/P molar ratio was first reported by Asada et al. [36]. The authors attributed this result to the formation of biphasic mixtures (HA–TCP) above 800 °C, but superficial diffusion at lower temperatures can be hypothesized. This mechanism can be particularly active when CaDHA powders are used for the sintering of BCP or TCP ceramics. Recently, Lukic et al. [37] showed that a faster heating rate resulted in a higher densification of BCP ceramics. They hypothesized that such an "unusual"[sic] behaviour could be due to the delayed formation of β-TCP when a fast heating rate was used. But, it should also be explained by less grain coalescence in CaDHA due to superficial diffusion in the early stage of sintering.

2.1.2. Intermediate and final stages of sintering: volume or grain boundary diffusion

At the end of the first stage of sintering, the ceramic body can be described as a skeleton of weakly bounded grains crossed by a network of open pores. Then, at higher temperatures from ~750 °C, the thermal energy supplied to the compact allows activation of volume or grain boundary diffusion of higher activation energy than superficial diffusion (~440 kJ mol^{-1} [35]). When densification begins, initial necks grow, forming grain boundaries [38], the total pore volume decreases and the sample shrinks (Fig. 1). At the same time, the total interfacial energy of grain boundaries ($dA_{ss}\gamma_{ss}$; Eq. (1)) also decreases by grain growth that occurs through grain boundary migration [39]. At the end of this second step, the ceramic body contains only residual closed pores (Fig. 5d). In the third and last step of sintering, closed pores may be reduced to ideally produce a fully dense ceramic.

The sintering mechanisms of HA was investigated by Landi et al. [19], who studied isothermal densification in the 940–1020 °C temperature range. For relative bulk density <85%, volume diffusion was predominant at low temperatures and for short times ($T < 1000$ °C, $t < 30$ min), whereas grain boundary diffusion was found at higher temperatures or for longer times. For higher relative density, the densification mechanism could not be identified in the last stage of sintering, because grain growth occurred simultaneously with densification.

The driving force of sintering due to interfacial energy also depends on surface curvature. Matter moves from convex ($r > 0$) to concave ($r < 0$) surfaces (Fig. 3a). This curvature contributes to grain boundary migration and grain growth. Ideally, a final equilibrium with flat grain boundaries should be reached. Using a simple two-dimensional model (more complex 3-D models exist, but they are not necessary in this paper), the final microstructure can be schematized by hexagonal grains with ideal equilibrium angles of 120° at the junction of three adjacent grains (see example in Fig. 11) [25,40].

Fig. 6 gives a tentative sintering map of HA, i.e. plot of grain size vs. the densification ratio, independently from sintering parameters. The methods used to measure the density and grain size are indicated in Tables 1–4. The Archimedes method is the most versatile for density measurement and is commonly used. Grain size is usually determined from scanning electron microscopy image analysis using either the linear intercept method or the equivalent disc diameter that has the same surface as the grain.

For better clarity, only some trajectories are drawn (Fig. 6a). Variability in the literature data is evidenced because experimental procedures (heating rate, temperature and time) change from one study to another (Table 1). More influential physical characteristics of green powder compacts (initial grain size, specific surface area, compaction ratio) may also vary in a wide range or are even not given in the available papers. Nevertheless, the main trends can be clearly defined:

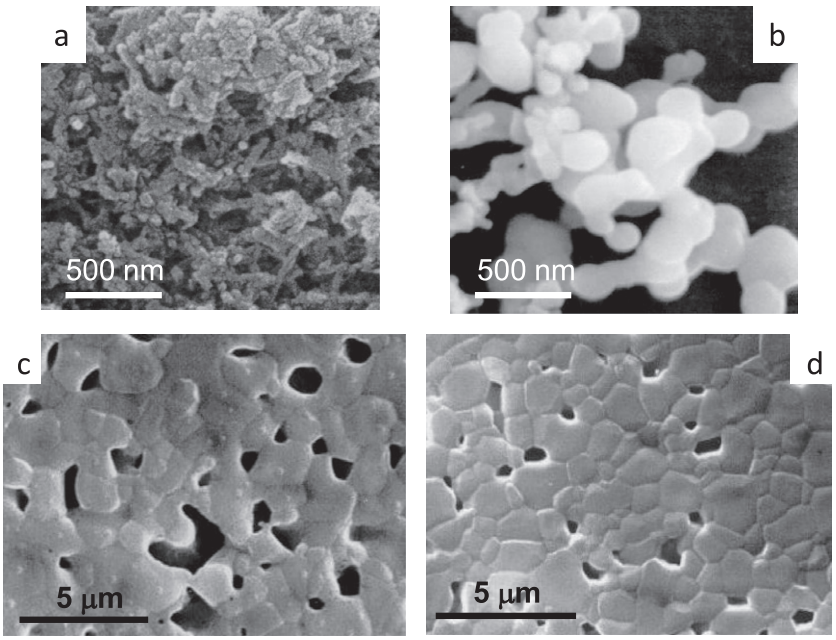

Fig. 5. Grain coalescence at low temperature in CaDHA after calcination at (a) 400 °C and (b) 700 °C [22]. (c) Typical microstructure of a BCP ceramic sintered from CaDHA powder with initial Ca/P = 1.535 (1250 °C, 30 min, ambient air) [22]. (d) Microstructure of pressureless sintered HA (1250 °C, 30 min, ambient air) [22].

(i) Pressureless sintering of HA to produce nearly fully dense ceramics (relative bulk density $\geqslant$98%) without significant grain growth (average grain size $\leqslant$1 μm) requires a temperature in the range 1100–1250 °C (Table 2). Lower temperatures do not allow the highest relative densities to be reached, and the highest temperatures promote grain growth (see temperature domains in Fig. 6b). As mentioned above, in this temperature range, only partial dehydroxylation may occur during sintering (Reaction (1)), leading to ceramics made of oxyhydroxyapatite [14,15,30]. Some authors reported on the effect of dehydroxylation on sintering. As it proceeds without apatite decomposition, it induces the formation of hydroxide vacancies (noted V^{o}_{OH}) and oxide ions O^{2-} (O'_{OH}) replace hydroxide ions OH^{-} (OH^{x}_{OH}). Thus, the dehydroxylation equilibrium (Reaction (1)) can be written as:

$$2OH^{x}_{OH} = O'_{OH} + V^{o}_{OH} + H_2O_{(gas)} \qquad \text{(Reaction2)}$$

Kijima and Tsutsumi [30] hypothesized that the creation of hydroxide vacancies increases reactivity and consequently enhances sintering. Royer et al. [15] showed that sintering modifies the dehydration process. In the last stage of sintering, when residual pores are closed, the weight loss due to dehydration stops. Exchanges with the atmosphere are then restricted to the surface. Therefore, the final OH stoichiometry of the bulk apatite depends on the pore closing temperature. A consequence of the dehydroxylation reaction during sintering at very high temperatures would be the creation of residual pores resulting from the release of H_2O gas that remains trapped inside the bulk material. This phenomenon can be hypothesized to explain a light decrease in density, often registered when an "optimal" temperature of densification is overshot (see solid line trajectories in Fig. 6a) [9,14,15,30,47,48]. The formation of fine pores was demonstrated by Liu and Chen in a recent paper [49] through annealing experiments of fully dense HA produced by SPS. When water vapour is trapped in closed pores during the last stage of sintering, it acts in what the authors called an "anti-densification process". Further densification is limited by water vapour diffusion through the bulk material near the surface. Finally, maximum densification depends on two main thermodynamic and kinetics parameters that are correlated: the temperature at which pores become closed and the advancement of HA dehydroxylation reaction at this temperature. Considering this last point, the sintering atmosphere should also play a role in the densification process. This is discussed in Subsection 2.1.3.

(ii) Grain growth in stoichiometric HA occurs mainly during the last stage of sintering, typically when relative bulk density is >95%, and it is particularly active at very high sintering temperatures, from ~1250 °C (Fig. 6b). This result agrees with the general behaviour of ceramic powder compacts during sintering. Grain growth, which usually occurs through grain boundary migration, is inhibited because of grain boundary pinning by the network of open pores in the intermediate stage of sintering [39]. In the final stage, the pinning phenomenon is drastically decreased, because only small residual closed pores are present, which enhances grain growth. Several authors calculated apparent activation energy (E_a) for grain growth during sintering. Values vary from 120 kJ mol^{-1} up to 240 kJ mol^{-1}. This variability can be explained partially by the varying stoichiometry of the investigated HA (i.e.Ca/P = 1.62 [10], 1.64 [35], 1.67 [9,44,50], 1.51 or 1.77 [47]). The kinetics of grain growth in CaDHA differs from that of stoichiometric HA, as evidenced from the dashed line trajectories in Fig. 6a. Moreover, these values of apparent activation energy E_a for grain growth are calculated from the slope of ln G (where G is the average grain size) vs. $1/T$, whereas it is formulated as follows in the case of normal grain growth [39]:

$$G^n - G_0^n = Kt\ \exp(-E'_a/RT) \qquad (3)$$

where G and G_0 are the average grain size after and before sintering, n is the kinetic grain growth exponent, which depends on the diffusion mechanism, T is the temperature, t is the time, E'_a is the "real" activation energy for grain growth, and K and R are constants.

According to this grain-growth model, grain size is temperature and time dependent. The grain size distribution must be similar for any period of time. In this hypothesis, the normalized distribution is invariant as a function of time [51] and the average grain size G can be used as a unique variable to characterize grain growth [52,53]. If the initial grain size G_0 can be neglected in Eq. (3), the

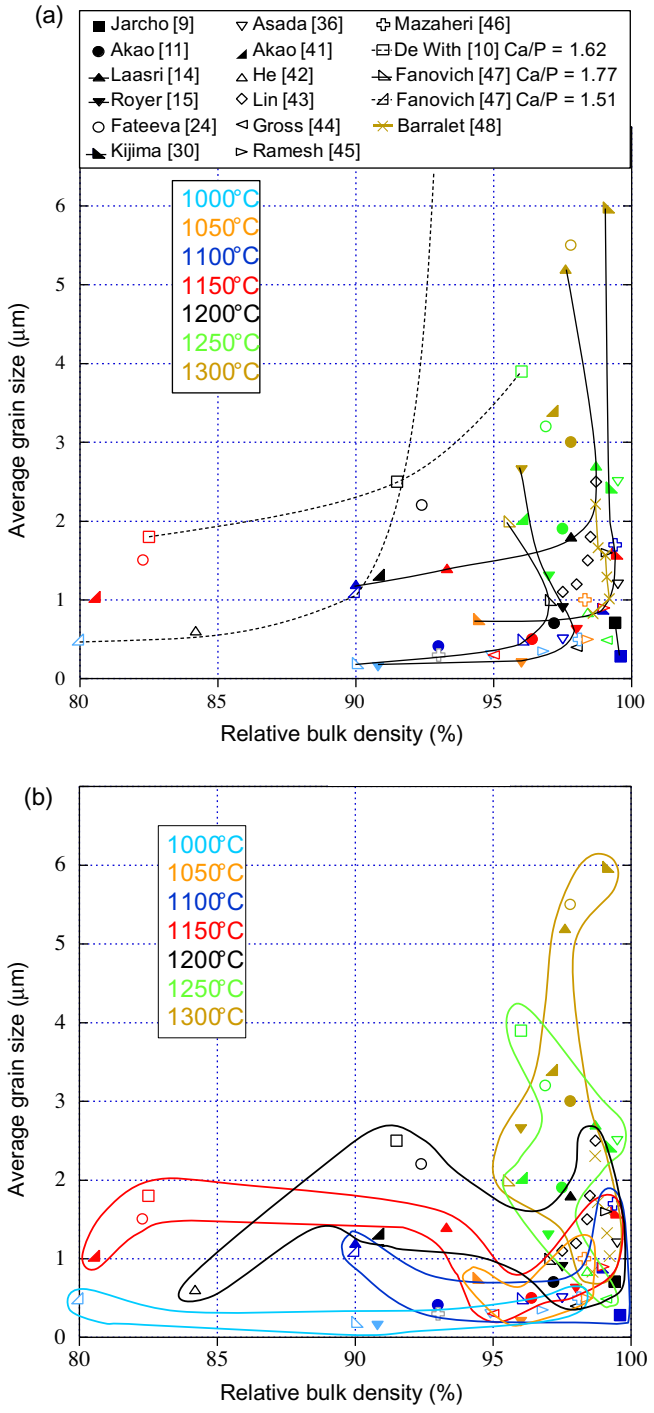

Fig. 6. (a) Pressureless sintering trajectories of HA and (b) data domains for a given sintering temperature.

apparent activation energy becomes $E_a = E'_a/n$. But the diffusion mechanism, i.e. the value of n, may change during sintering. This is the case when the system passes from the intermediate to the final stage of sintering at ~95% of relative density (Fig. 6b). These two domains, in which grain growth greatly differs, should be treated separately. Finally, the values of apparent activation energy E_a given in the literature should be taken with care, because they do not give the real activation energy E'_a.

Like maximum densification, grain growth depends on thermodynamic and kinetics parameters that also relate to the temperature at which pores become closed. But, as no study formally investigated grain growth kinetic vs. temperature in HA, it is difficult to conclude whether temperature or time is predominant (Table 2). Recently, a new type of sintering cycle, called "two-step sintering" (TSS) was investigated as a novel way to prevent grain growth during densification. It is detailed in Subsection 2.1.4.

2.1.3. Influence of sintering atmosphere

Vacuum [54,55], inert gas (N_2, O_2, Ar) [32,38,56,57], carbon dioxide [57] or moist air was used as the sintering atmosphere [10,37,44,54,57]. Generally, moisture was introduced in the sintering atmosphere to prevent dehydroxylation of HA (Reaction (1)). Some authors showed a slightly better sinterability of HA in vacuum than in air [54,55]. Conversely, sintering is delayed in moisture [54]. These results agree with the hypothesis that sintering would be enhanced by the creation of lattice vacancies resulting from the dehydroxylation of HA (Reaction (2)). Dehydroxylation is delayed by increasing the partial pressure of water vapour [58]. Similarly, as shown in Fig. 2, whereas there is no significant difference when ambient air or inert atmosphere is used, the presence of carbon dioxide delays sintering. This can be explained by a detrimental effect of A-type carbonate in HA (i.e. carbonate in the OH site of the apatite) on the diffusion of limiting species [57]. A-type carbonate results from the carbonation reaction that occurs from 800 °C during heating HA in a CO_2-containing atmosphere according to the reaction [59]:

$$Ca_{10}(PO_4)_6(OH)_2 + yCO_{2(gas)} \leftrightarrow Ca_{10}(PO_4)_6(OH)_{2-2y}(CO_3)_y + yH_2O_{(gas)} \quad \text{(Reaction3)}$$

It can be hypothesized that the mobility is reduced by A-site carbonation because of the great size and the more negatively charged carbonate ions.

Moisture may also affect grain growth. As detailed in Subsection 2.1.1, it promotes grain coalescence at low temperatures when superficial diffusion is active (Eq. (2)). It may result in CaP ceramics with coarse grains when starting from CaDHA powders, while it does not seem to have an effect when stoichiometric HA is sintered (see Refs. [10] and [44] in Fig. 6 and Table 1).

2.1.4. TSS

Grain growth occurs mainly during the final stage of sintering. Based on this fact, Chen and Wang [60] proposed a new sintering method called "two-step sintering" (TSS). This method consists of suppressing grain boundary migration responsible for grain growth, while keeping grain boundary diffusion that promotes densification. This would be effective in exploiting the difference in kinetics between grain boundary migration and grain boundary diffusion. Practically, a modified heating schedule, including two steps must be defined. In the first step, the sample has to be heated up to a temperature sufficiently high to reach a critical relative bulk density of ~70%. Then, it must be rapidly cooled and held at a lower temperature until densification is completed. This approach was applied by Mazaheri et al. for the sintering of HA ceramics [46]. The sintering data from this study are plotted in Fig. 7. (Experimental conditions for data from Fig. 7 are summarized in Table 3.) The average grain size remains slightly smaller than those of conventionally pressureless sintered HA ceramics, though the difference does not appear really significant (Table 2).

2.2. Liquid phase sintering of HA

In liquid phase sintering, the objective is to promote densification of HA and prevent grain growth by the presence of a liquid phase created from sintering additives. Two main mechanisms can be effective, viscous rearrangement or the dissolution–precipitation process [61,62].

Table 1
Experimental procedures for pressureless sintering trajectories of HA; data plotted in Fig. 6.

[Ref.] First author, publication year	Sintering conditions	Characteristics of initial powder				
	Atmosphere, temperature, time, heating rate	Preparation (supplier) Calcination	Composition Ca/P molar ratio	Average grain size G_0 (μm)	Specific surface area ($m^2\ g^{-1}$)	Green density Method (% d_{th})
[9] Jarcho et al., 1976	Air, 1100–1190 °C, 1 h, About 20 °Cmin^{-1}	Wet precipitation [LM], filtration	Stoichiometric HA 1.67	~0.02	DNA	Filtered cake + drying (DNA)
[10] De With et al., 1981	Moist oxygen, 1100–1250 °C, 6 h, 60 °C h^{-1}	Commercial powder (Merck, Germany)	HA + impurities (Mg, Na) 1.62	DNA	65	+5 wt.% H_2O CIP (50)
[11] Akao et al., 1984	Air, 1100–1300 °C, 1 h, DNA	Wet precipitation [LM], filtration 800 °C, 3 h + grinding	HA + 0.3 wt.% MgO DNA	DNA	DNA	+3 wt.% PVA UDP (DNA)
[14] Laasri et al., 2010	Air, 1000–1300 °C, 3 h, 5 °C min^{-1}	Wet precipitation [LM], washing Grinding in ethanol	Stoichiometric HA close to 1.67	0.1	90	+Dispersant Casting (55)
[15] Royer et al., 1993	Air, 1000–1300 °C, 5 h, 100 °C h^{-1}	Wet precipitation [LM], filtration Spray-drying + 800 °C, 5 h	Stoichiometric HA 1.667	DNA	18	CIP (>55)
[24] Fateeva et al., 2001	Air, 1100–1350 °C, 2 h, 4 °C min^{-1}	Wet precipitation [LM] 900–1000 °C + grinding in ethanol	HA 1.67	<2	4.4	+20 wt.% PVB UDP (63)
[30] Kijima et al., 1979	Air, 1050–1450 °C, 3 h, 15 °C min^{-1}	Wet precipitation [LM], washing 900 °C, 3 h	HA DNA	0.16	DNA	CIP (DNA)
[36] Asada et al., 1988	Air, 1000–1250 °C, 3 h, 500 °C h^{-1}	Wet precipitation [LM], washing	HA 1.665	DNA	DNA	Centrifugation + drying (DNA)
[41] Akao et al., 1981	Air, 1100–1300 °C, 4 h, DNA	Wet precipitation [LM], filtration 800 °C, 3 h + grinding	HA 1.69	DNA	DNA	UDP (DNA)
[42] He et al., 2008	Air, 1100–1250 °C, 2 h, DNA	Commercial powder (Merck, Germany)	Highly pure HA DNA	0.05–0.1	DNA	UDP (DNA)
[43] Lin et al., 1989	Air, 1200 °C, 1–10 h, 5 °C min^{-1}	Wet precipitation [LM], washing	Na-HA $Ca_{9.65}Na_{0.35}(PO_4)_6(OH)_{1.65}$	~0.06	29.9	UDP (51)
[44] Gross et al., 2004	Moist air, 1150–1250 °C, 2 h, 5 °C min^{-1}	Wet precipitation [LM], washing, 900 °C, 1 h + grinding in ethanol	HA DNA	0.15–0.35	9	CIP (DNA)
[45] Ramesh, 2008	Air, 1000–1300 °C, 2 h, 2 °C min^{-1}	Wet precipitation [LM], washing	HA 1.67	DNA	71.2	CIP (DNA)
[46] Mazaheri et al., 2009	Air, 800–1100 °C, 1 min, 0.1 °C s^{-1}	Commercial powder (Plasma Biotal Ltd., UK)	HA DNA	Rods 0.09 length and 0.025 width	DNA	CIP (51)
[47] Fanovich et al., 1998	Air, 1000–1300 °C, 1 h, 50 °C min^{-1} up to 800 °C,10 °C min^{-1} up to 1000 °C, 5 °C min^{-1} up to $T_{sintering}$	Commercial powder (Sigma Chem Co.) 500, 1000 °C	HA 1.77 1.51	DNA (agglomerates)	DNA	UDP (~50)
[48] Barralet et al., 2003	Air, 1300 °C, 0–24 h, 5 °C min^{-1}	Commercial powder (Plasma Biotal Ltd., UK)	HA	DNA	DNA	UDP (46)

DNA, data not available; CIP, cold isostatic pressing; UDP, uniaxial die pressing.
[LM] laboratory made.

Table 2
Sintering conditions and characteristics of nearly fully dense HA ceramics (relative bulk density ⩾98%) with fine grain size (⩽1 μm).

[Ref.] First author, publication year	Sintering conditions Atmosphere, heating rate (°C min^{-1}), temperature (°C), time	Characteristics of sintered ceramic	
		Relative density (%)	Average grain size G (μm)
[9] Jarcho et al., 1976	Pressureless sintering		
	Air, 20, 1100, 1 h	99.6[AM]	0.284[Li]
[15] Royer et al., 1993	Pressureless sintering		
	Air, 1.7, 1150, 5 h	98[AM]	~0.60[Li]
[30] Kijima et al., 1979	Pressureless sintering		
	Air, 15, 1100, 3 h	98.9[AM]	0.89[Li]
[42] He et al., 2008	Pressureless sintering		
	Air, DNA, 1250, 2 h	98.4[AM]	0.84
[44] Gross et al., 2004	Pressureless sintering		
	Moistair, 5, 1200, 2 h	98.0[AM]	0.40[Li]
	Moist air, 5, 1250, 2 h	99.1[AM]	0.49[Li]
[45] Ramesh et al., 2008	Pressureless sintering		
	Air, 2, 1100, 2 h	98.4[AM]	0.50[Li]
	Air, 2, 1150, 2 h	99[AM]	0.90[Li]
[46] Mazaheri et al., 2009	Pressureless sintering		
	Air, 6, 1000, 1 min	~98[AM]	~0.50[Li]
	Two-step sintering	98.8[AM]	0.19[Li]
	Air, 0.1 °C s^{-1}, 900 °C, 1 min, cooling 1 °C s^{-1} down to 800 °C, 20 h		
[48] Barralet et al., 2003	Pressureless sintering		
	Air, 5, 1300, 0 min	98.4[HP]	0.90[Li]
	CO_2, 5, 1300, 0 min	99.3[HP]	0.65[Li]
[12] Halouani et al., 1994	HP—20 MPa (graphite die)		
	Argon, 15, 1100, 30 min	98.8[AM]	0.20[Li]
	Argon, 15, 1200, 30 min	99.5[AM]	0.40[Li]
[74] Raynaud et al., 2002	HP—20 MPa (graphite die)		
	Argon, 20, 1200, 30 min	98.9[AM]	0.40[ED]
[77] Hirayama et al., 1987	Post-HIP—196 MPa		
	Argon, DNA, 1050, 4 h	99.8[AM]	0.32[Li]
[78] Wakai et al., 1990	Post-HIP—203 MPa		
	Argon, DNA, 1000, 2 h	99.9	0.64[Li]
[79] Takikawaet al., 1996	Post-HIP—200 MPa		
	Argon, DNA, 1100, 1 h	99.6[GM]	0.42[Li]
[80] Uematsu et al., 1989	HIP—100 MPa (glass capsule sealed under vacuum at 600 °C)		
	–, 800–1000, 2 h	100[AM]	~0.10
[91] Nakahira et al., 2003	SPS—30 MPa (graphite die) Argon, 100, 700, 5 min		
	Argon, 100, 800, 5 min	99.2[AM]	0.30
		98.5[AM]	0.80
[92] Guo et al., 2005	SPS—50 MPa (graphite die)		
	Vacuum, 100, 825, 3 min	98.6[AM]	0.13 length–0.098 width
	Vacuum, 100, 950, 1 min	98.4[AM]	0.21 length–0.17 width
[131] Chaudhry et al., 2011	SPS—100 MPa (graphite die)		
	DNA, 200, 1050, 3 min	100 (traces TCP)	0.221
[133] Wang et al., 2007	Pressureless sintering		
	Air, DNA, 900, 2 h	99.4[AM]	0.083

DNA, data not available.
[AM] Archimedes method.
[GM] geometrical measurement and weighing.
[HP] helium pycnometry.
[Li] linear intercept method.
[ED] equivalent disc diameter.

Table 3
Experimental procedures for sintering trajectories of HA ceramics; data plotted in Fig. 7.

[Ref.] first author, publication year	Sintering conditions	Characteristics of initial powder				
	Temperature, time, atmosphere, stress, heating rate	Preparation (supplier) Calcination	Composition Ca/P ratio	Average grain size G_0 (μm)	Specific surface area ($m^2\,g^{-1}$)	Green density Method (% d_{th})
[46] Mazaheri et al., 2009	TSS 0.1 °C s^{-1} up to 900 °C, 1 min cooling 1 °C s^{-1} down to 800 °C, 0–20 h, air	Commercial powder (Plasma Biotal Ltd., UK)	HA DNA	Rods 0.09 length and 0.025 width	DNA	CIP (51)
[12] Halouani et al., 1994	HP 1000–1250 °C, 30 min, argon, 20 MPa 15 °C min^{-1}	Commercial powder (Bioland, France)	HA 1.67	0.045	23.5	Powder DNA
[74] Raynaud et al., 2002	HP 1100–1120 °C, 30 min, argon, 20 MPa 20 °C min^{-1}	Wet precipitation[LM], filtration	HA 1.667	Rods 0.10 length	58	Powder DNA
[75] Veljović et al., 2009	HP900–1000 °C, 1–2 h, argon, 20 MPa	Wet precipitation[LM] Spray-drying	HA 1.67	Rods 0.50–0.10 length	59	CIP (60)
[77] Hirayama et al., 1987	Pressureless presintering 960 °C, 2 h, vacuum Post-HIP, 1050 °C, 4 h, argon, 196 MPa	Wet precipitation[LM] Calcination + grinding	HA	DNA	DNA	CIP (DNA)
[78] Wakai et al., 1990	Pressureless presintering 1050 °C, 2 h, air Post-HIP 1000 °C, 2 h, argon, 203 MPa	Wet precipitation[LM]	HA 1.67	DNA	DNA	CIP (DNA)
[79] Takikawa et al., 1996	Pressureless presintering 1100 °C, 2 h, air Post-HIP 1100 °C, 1 h, argon, 200 MPa	Wet precipitation[LM] 800 °C, 1 h + grinding	HA	DNA	DNA	+3.5 wt.% PVA UDP (DNA)
[91] Nakahira et al., 2003	SPS 700–1200 °C, 5 min, argon, 30 MPa, 100 °C min^{-1}	Commercial powder (Taihei Chemical Co., Jpn)	HA	DNA	37	Powder DNA
[93] Eriksson et al., 2011	SPS 700–1200 °C, 5 min, vacuum, 30 MPa, 100 °C min^{-1}	Wet precipitation[LM]	HA	Rods 0.45 length, 0.18 width	45	Powder DNA

DNA, data not available; CIP, cold isostatic pressing; UDP, uniaxial die pressing.
[LM] laboratory made.

2.2.1. Viscous flow of intergranular glassy phase allowing HA grain rearrangement, therefore favouring porosity elimination

This approach has been used for processing glass reinforced HA matrix composites with enhanced mechanical or biological performances [63–66]. Various glass compositions were studied in the system SiO_2–P_2O_5–CaO–Na_2O. The addition of glass retards densification [67,68] and grain growth [63–65]. Nevertheless, it is difficult to conclude unambiguously on this last point because, in these studies, grain sizes are given vs. the sintering temperature, and there are no available data relating grain size to the relative density of sintered samples in order to build up sintering maps. Sintering is performed at very high temperatures (i.e.1200–1350 °C for at least 1 h) and HA transforms partially into TCP. The mechanism by which TCP is formed is not clearly described, but its presence is hypothesized to originate a strengthening of the material. When the glass composition contains sodium, other crystalline phases, such as $CaNaPO_4$ or $CaSiO_2$, can be formed during sintering [66]. The authors hypothesized that sodium would diffuse into the HA structure, inducing HA transformation into $CaNaPO_4$, while $CaSiO_2$ would nucleate in the glassy phase.

2.2.2. Formation of a eutectic with HA, allowing interface dissolution of HA in the liquid, matter diffusion through the liquid and redeposition onto the grain surfaces

This mechanism requires the existence of a eutectic composition between the additive and CaP. Among the known binary systems, Li_3PO_4 (in the composition 60 wt.%) forms a eutectic at 1010 °C with $Ca_3(PO_4)_2$ [69]. From this basis, alkali cations, lithium Li^+ (in the form of phosphate Li_3PO_4 [69], carbonate Li_2CO_3 [70] or nitrate $LiNO_3$ [47,71]) and sodium Na^+ (in the form of metaphosphate $NaPO_3$ [70] or phosphate Na_3PO_4 [24,70]) were investigated.

Addition of lithium enhances densification. It provokes the partial decomposition of HA with formation of β-TCP at ~900 °C below the eutectic point. A possible decomposition reaction of HA can be deduced from the work of Ababou and Bernache-Assollant [70] when $Li_2CO_3$is used:

$$Ca_{10}(PO_4)_6(OH)_2 + 3Li_2CO_3 \rightarrow 2Li_3PO_4 + 2Ca_3(PO_4)_2 + 4CaO + 3CO_2 + H_2O \quad \text{(Reaction 4)}$$

Then, a liquid phase can form by reaction of TCP with lithium phosphate at 1010 °C.

Addition of $NaPO_3$ leads to a reaction that results in the formation of β-TCP, but there is no evidence for the formation of any liquid phase [70].

Sodium phosphate Na_3PO_4 seems to be an effective additive to enhance sintering of HA. A shift of ~50 °C to lower temperatures is observed in the presence of Na_3PO_4 [24]. But the additive does not seem to affect grain growth strongly. This would agree with the work of Santos et al. [65], who indicated that there was no evidence for any control of grain size by the glassy phase (in the system SiO_2–P_2O_5–CaO–Na_2O) during sintering. Nevertheless, this hypothesis must be taken with care, because very few results are available. The formation of $CaNaPO_4$ is always observed after cooling to room temperature [24,70], and the lattice parameters of HA change, indicating partial substitution of Na for Ca in the crystal structure. The following mechanism is proposed [70]:

$$Ca_{10}(PO_4)_6(OH)_2 + xNa_3PO_4 \rightarrow Ca_{10-x}Na_x(PO_4)_6(OH)_{2-x} + 2xCaNaPO_4 + 2xNa_2O + xH_2O \quad \text{(Reaction 5)}$$

Suchanek et al. [72] investigated numerous sintering additives. H_3BO_3, $CaCl_2$, KCl, KH_2PO_4, $(KPO_3)_n$ and $Na_2Si_2O_5$ did not enhance densification and induced the formation of secondary phases. K_2CO_3, Na_2CO_3 and KF enhanced densification by formation of a liquid phase, but β-TCP or CaO were formed. These sintering aids form a liquid phase at low temperature that favours grain

Table 4
Sintering conditions and characteristics of TCP and BCP ceramics.

[Ref.] First author, publication year	Powder preparation (supplier)	Sintering conditions	Characteristics of initial material (Ca/P, average grain size G_0)	Characteristics of sintered ceramics		
				Phase composition	Relative density (%)	Average grainsize G (μm)
[13] Destainville et al.,[a] 1994	Wet precipitation[LM] Filtration 740 °C, 30 min	HP 900–1100 °C, 30 min, 20 MPa	β-TCP (Ca/P = 1.50)	β-TCP (T = 1050 °C)	99.7[AM]	0.65[ED]
[107] Bandyopadhyay et al., 2007	Commercial powder (Monsanto, CA) Ball milled, 5 h + UDP	Pressureless sintering 1250 °C, 3 h, air	TCP TCP + 2.5 wt.% ZnO	TCP (α or β not specified) TCP (α or β not specified)	89.3[GM] 94[GM]	9.7 1.9
[144] Akao et al.,[a]1982	Wet precipitation[LM] Filtration, 800 °C for 3 h + grinding + 1 wt.% corn starch + UDP	Pressureless sintering 1100–1300 °C, 1 h, air	Apatite (Ca/P = 1.51) apatite (Ca/P = 1.51)	β-TCP (T = 1200 °C) β-TCP + HA (T = 1250 °C)	99.4 DNA	1.59 ± 0.69[Li] 2.23 ± 0.94[Li]
[147] Zhang et al., 2008	Wet precipitation[LM] Washing + 10 wt.% PVA + 800 °C for 2 h	SPS 880 °C, 3 min, vacuum, 50 MPa	β-TCP (G_0 = 80 nm)	β-TCP	99[AM]	~0.2
[148] Douard et al., 2011	Wet precipitation[LM] Washing, 750 °C for 30 min + UDP	Pressureless sintering 1100 °C, 2 h, air	β-TCP (Ca/P = 1.51) β-TCP + 0.95 wt.% Si	β-TCP β-TCP + amorphous silicon rich phase	99.7[AM] 98.0[*,AM]	1.60 ± 0.69[ED] 0.50 ± 0.20[ED]
[149] Itatani et al., 1994	Spray pyrolysis[LM] Grinding, 600 °C for 1 h	Pressureless sintering 1070 °C, 5 h, air	β-TCP + HA	β-TCP	96.1	DNA
[150] Tampieri et al., 1997	Commercial powder (Jesse-Shirley, UK)	Pressureless sintering 1220–1260 °C, 1 h, air HP 1150 °C, 1 h, 30 MPa	HA + $CaHPO_4$ 1:1 M HA + $CaHPO_4$ 1:1 M	β-TCP + α-TCP + HA β-TCP + 10 vol.% HA	91–92.2[AM] 100[AM]	DNA ~1–2
[152] Jarcho et al.,[a]1979	Wet precipitation[LM] Washing, 750 °C for 30 min	Pressureless reaction sintering 1000–1250 °C, 1 h then 4 h at 990 °C	Sulfate doped TCP	β-TCP (T = 1200 °C)	99.7[AM]	0.483
[153] Ryu et al., 2002	Solid-state reaction at 1100 °C + ball milled for 24 h in ethanol, CIP	Pressureless sintering 1200 °C, 2 h, air	β-TCP β-TCP + 0.5–3 wt.% $Ca_2P_2O_7$	β-TCP + 42% α-TCP β-TCP	~87[*,AM] > 95[AM]	DNA DNA
[155] Carbajal et al., 2012	Solid-state reaction at 900 °C, 2 h + attrition + CIP	Pressureless sintering 1100–1250 °C, 12 h, air	β-TCP β-TCP + 0.25 wt.% ZnO	β-TCP + α-TCP (T = 1100 °C) β-TCP + α-TCP (T = 1250 °C)	90[AM] 92[AM]	DNA DNA
[156] Xue et al., 2008	Wet precipitation[LM] Filtration + grinding + 650 °C, for2 h + UDP	Pressureless sintering 1250 °C, 2 h, air	TCP TCP + 1 wt.% MgO TCP + 0.3 wt.% ZnO TCP + 1 wt.% MgO + 0.3 wt.% ZnO	β-TCP + α-TCP β-TCP β-TCP + α-TCP + glassy phase β-TCP	82[AM]92.9[AM]91.8[AM]99.3[AM]	DNADNADNADNA
[157] Banerjee et al., 2010	Commercial powder(Berkeley Advanced Biomaterials Inc., CA) + milled for 6 h + UDP	Pressureless sintering 1250 °C, 2 h, air	β-TCPβ-TCP + 1 wt.%MgO + 2 wt.% SrO	β-TCP + α-TCPβ-TCP	96.17[AM]97.26[AM]	2.62 ± 0.142.33 ± 0.18
[158] Fielding et al., 2012	Commercial powder(Berkeley Advanced Biomaterials Inc., CA) + milled for 6 h + 3-D printing with binders	Pressureless sintering1250 °C, 2 h, air	β-TCPβ-TCP + 0.25 wt.% ZnO + 0.5 wt.% SiO_2	β-TCP + α-TCPβ-TCP + α-TCP	90.8 ± 0.8[AM]94.1 ± 1.6[AM]	DNADNA
[159] Seeley et al., 2007	Commercial powder(Berkeley Advanced Biomaterials Inc., CA) + milled for 6 h + UDP	Pressureless sintering1250 °C, 4 h, air	β-TCPβ-TCP + 1 wt.% TiO_2β-TCP + 0.5 wt.% Ag_2O	β-TCP + α-TCP + HAβ-TCP + α-TCP + HAβ-TCP + α-TCP + HA	66[*,GM]81[*,GM]68[*,GM]	35.63
[160] Seeley et al., 2008	Commercial powder(Berkeley Advanced Biomaterials Inc., CA) + milled for 6 h + UDP	Pressureless sintering1250 °C, 4 h, air	β-TCP + 2 wt.% NaFβ-TCP + 3 wt.% CaO	β-TCP + α-TCP + HAβ-TCP+α-TCP+HA	80[*]~67[*]	7.176.63
[36] Asada et al.,[a]1988	Wet precipitation[LM] Washing	Pressureless sintering 1000–1250 °C, 3 h, air, 500 °Ch^{-1}	CaDHA (Ca/P = 1.64)	BCP (95 wt.% HA + 5 wt.% TCP)T = 1250 °C	97[GM]	0.6
[74] Raynaudet al., [a]2002	Wet precipitation[LM] Filtration	HP 1100–1200 °C, 30 min, Ar, 20 MPa, 20 °C min^{-1}	CaDHA (Ca/P = 1.617)	BCP ((71 wt.% HA + 29 wt.% TCP)T = 1100 °CT = 1200 °C	99[AM]98.8[AM]	0.25[ED]0.8[ED]

DNA, data not available; UDP, uniaxial die pressing; CIP, cold isostatic pressing.
[LM] laboratory made.
[AM] Archimedes method.
[GM] geometrical measurement and weighing.
[Li] linear intercept method.
[ED] equivalent disc diameter.
[*] Normalized to the theoretical density of β-TCP (3.07 g cm^{-3}).
[a] Sintering trajectory plotted in Fig. 9.

rearrangement during the early stage of sintering. The creation of OH vacancies (V^{o}_{OH}) due to K^{+} or Na^{+} substitution for Ca^{2+} in the HA lattice may also contribute to better sinterability by facilitating solid-state matter diffusion. Only mixtures of sodium phosphates with atomic ratio (Ca + Na)/P = 1.67 appeared effective and did not form a secondary phase. This could be explained by the formation of Na-substituted HA $Ca_{10-x}Na_x(PO_4)_6(OH)_{2-x}$ for this particular value of (Ca + Na)/P molar ratio. But no liquid phase was observed with this additive, so that the better sinterability was attributed to the formation of OH vacancies in the Na-substituted HA. This case corresponds rather to the solid-state sintering of a substituted HA.

Finally, the liquid phase sintering of HA with additives always leads to the formation of secondary chemical compounds either amorphous or crystalline.

2.3. Solid-state assisted sintering of HA

From the beginning of the 1980s, several authors attempted to use "physically" assisted sintering techniques. Thus, HP, HIP, MWS and, more recently, SPS or ultrahigh-pressure sintering (UHP) have been investigated. All these techniques provide an additional driving force (pressure, electric/magnetic field) that is expected to promote densification and prevent grain growth by decreasing sintering temperature and/or time. The main objective is to improve the mechanical reliability of HA itself by producing fully dense ceramics with fine grains or by incorporation of a second ceramic phase in the HA matrix. In this last case, assisted sintering appears necessary, because the presence of a second phase drastically slows down or inhibits sintering of the HA matrix. This phenomenon is well known in ceramic–ceramic composites when inert reinforcing inclusions (particles, fibres or platelets) are used [73]. The sintering of CaP matrix based composites will not be detailed here, only the influence of additional pressure (HP, HIP, UHP), electrical field and pressure (SPS) or microwaves on the sintering of HA is presented.

2.3.1. HP, HIP and UHP

HP and UHP allow application of a mechanical uniaxial compressive stress on the sample. They require the use of a die, which limits the possible shapes of samples. In HIP, a gas pressure is isostatically transmitted to the sample encapsulated in a deformable container, which allows sintering of complex shapes. Very few studies have been devoted to the sintering of pure HA by HP or HIP. So, only partial results are available.

Data for hot-pressed HA are given in Fig. 7 [12,74,75]. The apparent activation energy for grain growth during HP was 122 kJ mol^{-1} [12]. A first attempt to densify HA by HIP, using the encapsulation technique was published in 1982 [76]. Two powdery samples were sealed in gold capsules, and 2.7 wt.% water was added to one capsule. HIPing was then performed at a very low temperature (i.e.550 °C for 3 h under 140 MPa), which resulted in HA ceramics with 74% and 71% of relative bulk density without and with water addition, respectively. Because the use of a gas pressure requires encapsulation of green compacts (generally in glass capsules and under vacuum), an alternative post-HIP method has been investigated. It includes initial pressureless sintering to reduce porosity, followed by post-HIPing without encapsulation. Sintering trajectories are also plotted in Fig. 7 [77–79]. (Associated experimental parameters are given in Table 3.)

In comparison with pressureless sintering, HP or HIP allows very high relative densities to be reached with limited grain growth due to lower sintering temperature and time (Table 2). This is the reason why HIP was used to produce transparent HA ceramics [80,81]. Such optical properties require pore-free material with very small grain size. For this reason, Tan et al. [82] used a low-temperature ultrahigh-pressure method (ULTHP), i.e.an alternative HP method performed under very high pressure (2–5 GPa), to produce nearly fully dense transparent HA ceramics with fine microstructure (average grain size $G \approx 200$ nm) at a temperature of only 435 °C under a pressure of 3 GPa.

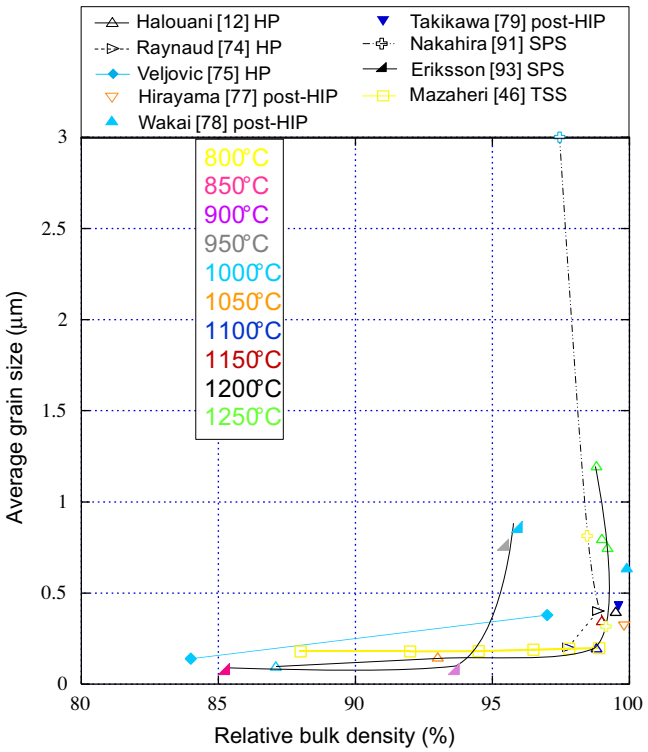

Fig. 7. Trajectories for assisted sintering of HA.

2.3.2. Microwave sintering

Microwave sintering of ceramics differs from conventional sintering because the heat is generated internally within the material by electromagnetic radiation instead of originating from an external source [83]. This provides numerous advantages, among which are reducing the temperature and time by fast heating and therefore obtaining ceramics with fine grains [84]. Fang et al. [85,86] first investigated MWS of HA at the beginning of the 1990s. They produced either porous or dense material. At 1200 °C, the grain size of HA conventionally sintered for 2 h was close to that measured after 10 min of MWS at the same temperature (~1 µm). But, the sintered density was slightly higher using MWS [86]. The authors hypothesized that hydroxide ions in HA might have played an important role in enhancing densification. The highest relative density reached ~95% after MWS at 1300 °C for 10 min, but important grain growth occurred, the average size reaching 3 µm. Other works gave somewhat similar results [45,87,88]. Relative density increased from ~87.5% to 94.5% with increasing MWS temperature from 900 to 1200 °C (15 min holding time). At the same time, grain size increased from 0.24 µm to 1.59 µm [87]. Ramesh et al. [45] used MWS at very high temperatures (1300 °C) to obtained ceramics with 98% relative density and an average grain size of 2 µm. Most of the published papers concluded that MWS was efficient when applied to HA ceramics. But, from these results, it appears that MW sintered ceramics hardly reach a relative density above 95% with grain size >1 µm, which is worse than pressureless sintering (Table 2). Moreover, as grain growth occurs mainly above this relative density (see sintering trajectories in Fig. 6a) conventional pressureless sintering remains obviously superior to MWS.

2.3.3. SPS

SPS is a "flash sintering method" in which an electric current is applied simultaneously with a compressive stress to a die containing the initial powdery sample [89]. In this respect, it resembles HP, but the sample is directly heated by the applied electric current, which results in very rapid and efficient heating. This technique should present numerous advantages over conventional sintering (faster heating rate and heat transfer as for MWS with application of a mechanical compressive stress). It is expected to lower temperature and shorten the holding time required for densification and, consequently, to overcome the problem of grain growth in nanostructured materials. Moreover, the electric current in SPS can also create polarization, a process that usually requires post-sintering operating [101], thus combining two processes into one.

Several authors have investigated SPS of pure HA to produce dense HA ceramic pellets with enhanced mechanical and/or biological properties [90–92], transparent ceramics [93,94] or as post-sprayed treatment of HA coatings [95]. Fig. 7 gives trajectories for SPS of HA drawn from available data. As for conventional pressureless sintering, grain growth is effective when the relative density reaches 95%. Apparent activation energy of grain growth was found to be 184 kJ mol^{-1} [90], which is of the same order of magnitude as that for pressureless sintering or HP. SPS allows for the production of nanostructured HA ceramics with microstructures similar to those obtained by HP or HIP. The main differences are that a lower temperature (~800 °C against 1000 °C) and much shorter holding times (~5 min against >30 min) are necessary. At very high temperatures (1200 °C), SPS leads to important *c*-axis growth of HA crystals, resulting in coarse acicular grains [91,94] that tend to lie in planes perpendicular to the direction of the applied compressive stress [94]. This phenomenon is encountered during uniaxial compressive stress assisted sintering (HP) of ceramic materials with hexagonal crystal structure [96], and it was also observed after ULTHP of HA [82].

Though the effect of pulsed electric current on the sintering mechanisms of HA is not clearly understood, SPS appears to be an interesting method of producing nanostructured dense HA ceramics. But, because of the applied compressive stress, limitations similar to those encountered with HP arise. The gain in grain size (~100–300 nm vs. ~400 nm for pressureless sintering; Table 2) cannot lead to subsequent improvement of the mechanical properties of HA that remain a critical factor, especially concerning the fracture toughness, which hardly reaches 1.5 MPa $m^{1/2}$. Nevertheless, SPS appears very promising for consolidation at very low temperatures of CaP ceramics made of thermally unstable calcium nanoparticles, such as nanocrystalline apatites, whose behaviour is detailed in Section 4.

3. Sintering of substituted HA

Numerous ions or ionic groups can enter the crystal structure of apatite, which gives rise to a great family of chemical compounds. Several ionic substitutions of biological interest in HA have been investigated. These substitutions may change the thermal stability and sintering behaviour of HA. Particular attention is given here to the substitution by carbonate, fluoride or silicate anions. To a much lesser extent, the production of HA ceramics substituted or co-substituted by various cations such as magnesium [97–101], strontium [101–106], zinc [99,101,107], bismuth [108], potassium [109] or yttrium [110] has been reported. The sintering of these metallic (co)-substituted HA also remains only partially investigated. Moreover, in most studies, the sintering is performed at very high temperatures (⩾1250 °C) or using HA of uncontrolled stoichiometry, which leads to thermal decompositions and multiphasic ceramics.

Thus, Mg was found to favour the thermal decomposition of HA into a biphasic mixture of HA and TCP [97,98]. The decomposition temperature decreases with increasing Mg content from 840 °C for 0.6 wt.% down to 660 °C [97] or even 300 °C [111] for 2.4 wt.%. This can be explained by the much smaller ionic radius of Mg^{2+} in comparison with Ca^{2+}, which implies that only a very low amount of Mg can substitute for Ca in the HA lattice (i.e. 0.4 wt.% according to [112]). Co-substitution of a second ionic species (carbonate [98] or silicate [100]) was investigated in order to introduce additional structural changes that may stabilize Mg substitution. This allowed an increase in the thermal stability of co-substituted HA containing up to 1 wt.% of Mg up to 1200 °C and to sinter without thermal decomposition.

The case of strontium is different, since it can fully substitute for calcium in the apatite lattice. Sr-subsituted HA was heated up to 1250 °C without thermal decomposition [103], but the sintering behaviour was not detailed. In another study, HA was doped with SrO [101], but the stoichiometry of HA powder was not controlled, which led to biphasic HA–TCP materials after sintering at 1200 °C. This was also the case when ZnO was used as HA dopant [101,107].

Finally, it is difficult and speculative to state a clear interpretation from these literature data, each case must be seen as particular. The sintering of these CPC will not be detailed.

3.1. Carbonated hydroxyapatite (CO_3-HA)

Carbonate (CO_3^{2-}) can substitute either for OH^- in the so-called "A site" of HA $Ca_{10}(PO_4)_6(OH)_{2-2y}(CO_3)_y$ or for PO_4^{3-} in the "B site" of HA $Ca_{10-x}(PO_4)_{6-x}(CO_3)_x(OH)_{2-x}$. These substitutions lead to a general chemical formula for AB-type carbonated hydroxyapatite (CO_3-HA): $Ca_{10-x}(PO_4)_{6-x}(CO_3)_x(OH)_{2-x-2y}(CO_3)_y$ [57].

B-type carbonation, generally measured using C–H–N elemental analysis, can be achieved during the synthesis of powder by wet chemical precipitation [57,113,114]. The difficulty in the sintering of carbonated HA is to prevent B-type decarbonation that occurs at low temperatures, from ~600 °C [115,116]. A CO_2-gas-containing atmosphere is required [57,114,117,118]. The thermal stability of B-type CO_3-HA depends on the temperature, the CO_2 gas pressure and the B-type carbonate content (i.e. the value of x) and can be predicted from thermodynamic calculations [119]. This allows the stability domain to be defined at equilibrium, and the maximum temperature at which sintering would be possible without degradation of the initial CO_3–HA to be predicted. For example (Fig. 8; note that the plots of this figure should not be confused with an experimental plot obtained from heated samples), in pure CO_2 flowing gas (P_{CO_2} − 1 bar), a B-type CO_3-HA containing x = 0.4 mol of carbonate would remain stable up to 1100 °C, whereas this temperature would only be 800 °C in air ($P_{CO_2} \approx 0.4 \times 10^{-3}$ bar). The thermal stability decreases with increasing carbonate content. Similarly, the experimental sintering temperature also decreases with B-type carbonation (Fig. 1) [57,117]. These results can be linked to the concentration of ionic vacancies (V_{OH}^{o} and V_{Ca}'') within the apatite lattice created by the B-type carbonate substitution, which favours matter mobility by diffusion.

Additionally, A-type carbonation occurs by exchange with hydroxide ions when heating in carbon dioxide atmosphere according to the following chemical equilibrium:

$$Ca_{10-x}(PO_4)_{6-x}(CO_3)_x(OH)_{2-x} + yCO_{2(gas)} \leftrightarrow Ca_{10-x}(PO_4)_{6-x}(CO_3)_x \times (CO_3)_x(OH)_{2-x-2y}(CO_3)_y + yH_2O_{(gas)} \quad \text{(Reaction 6)}$$

The composition of the A site (value of *y*) depends on the temperature and pressures of CO_2 and H_2O. It can be calculated at the thermodynamic equilibrium from the equilibrium constant of Reaction (6) [57,120]. So, in addition to CO_2 gas, a partial pressure of water vapour in the atmosphere is helpful to control A-site

composition. While B-type carbonation decreases the sintering temperature, A-type carbonation induces a light shift to higher sintering temperatures (see Fig. 2, HA in CO_2 atmosphere). Finally, AB-type CO_3-HA ceramics with controlled composition and fine grains can be fully sintered at low temperatures ($T \leqslant 900\ ^\circ C$) in mixed flowing atmospheres containing partial pressures of CO_2 and H_2O vapour [57,114,117].

3.2. Hydroxyfluorapatites

Fluoride ions can substitute for hydroxide in the apatite lattice. Thus, hydroxyfluorapatites (F-HA) have the chemical formula $Ca_{10}(PO_4)_6(OH)_{2-x}F_x$. The sintering of F-HA differs slightly from that of pure HA. It appears much more complex to analyse because it depends on the fluoride content, with equal amounts of fluoride and hydroxide ions ($x \approx 1$) observed to greatly reduce the sintering [44,121]. Gross and Rodriguez-Lorenzo attributed this behaviour to hydrogen bonding between more electronegative fluoride ions and hydroxide ions, which would decrease the mobility of these species [44]. It is also in agreement with a densification mechanism controlled by the mobility of species present in the hydroxyl columns of apatites. Similarly, hydroxide vacancies enhance the diffusion, whereas A-type carbonates lower it (see Subsection 2.1). For $x < 1$ or $x > 1$, the behaviour resembles that of pure HA. Only a slight decrease in the densification can be noticed with increasing fluoride content, while grains grow more [44]. Gross and Bhadang also studied the sintering of biphasic mixtures of hydroxyapatite and fluorapatite [122]. A single F-HA solid solution was formed from the biphasic mixture. The hypothesized sintering mechanism is the same as that stated for the sintering of F-HA solid solutions [44], implying the mobility of F^- and OH^- ions in the hydroxyl column. But, with the use of biphasic mixtures, the sintering rate was lower, owing to reduced mobility within the interfacial zones between hydroxyapatite and fluorapatite particles.

Though the sintering behaviour of F-HA remains little documented and not totally clear, the above studies indicate that, in the presence of fluoride ions, volume or grain boundary diffusion is less active than grain boundary motion.

As for HA or A-type CO_3-HA, the atmosphere can influence the sintering of F-HA. Though its effect on densification has not been quantified, a wet atmosphere may induce volatilization of fluoride according to the following reaction [123]:

$$Ca_{10}(PO_4)_6F_2 + xH_2O \leftrightarrow Ca_{10}(PO_4)_6(OH)_xF_{2-x} + xHF \quad \text{(Reaction 7)}$$

This reaction does not create vacancies in the apatite lattice, but changes the fluoride stoichiometry.

3.3. Silicon substituted hydroxyapatite (Si-HA)

Silicon can substitute for phosphorus in the HA lattice, leading to the chemical formulae $Ca_{10}(PO_4)_{6-x}(SiO_4)_x(OH)_{2-x}$. A typical shrinkage plot of Si-HA powder compact vs. the temperature is given in Fig. 1. The general trend is that silicon substitution decreases the sinterability of HA [23,100,124–126]. T_M shifts to higher temperatures as the silicon content increases (Fig. 2) [23,126]. Densification of Si-HA requires higher temperatures than HA. But, at the same time, the presence of silicon also reduces grain growth [23,35,124]. A difficulty comes from the fact that the temperature of thermal decomposition of Si-HA decreases with the increase in silicon content (Fig. 9). This decomposition leads to α-TCP and/or silicocarnotite $Ca_{10}(PO_4)_4(SiO_4)_2$ [23,100,125]. From the literature data, it appears hardly feasible to fully sinter Si-HA containing high amounts of silicon without decomposition. Dense (relative density >95%) and single phase Si-HA ceramics containing up to a limit of ~0.5 mol of silicon (i.e. 2 wt.%) with a fine microstructure ($G \approx 0.5\ \mu m$) have been produced within the thermal stability region (Fig. 9) [23,100,127].

Some authors attempted to analyse the mechanisms of sintering of Si-HA. From the calculation of activation energies, Putlayev et al. [35] stated that silicon would slow down the formation of contacts between particles, owing to reduced grain boundary mobility during the first stage of sintering. Then, in the second stage of sintering, silicon would promote densification through grain boundary diffusion enhanced by the formation of hydroxide vacancies in the Si-HA lattice. This interpretation is based on the calculation of activation energies from shrinkage curves. Gibson et al.'s [124] hypotheses are more complex. The changes in electric charges due to the substitution of PO_4^{3-} by SiO_4^{4-} ionic groups could greatly modify binding energies and interaction forces between ionic groups in the HA lattice. This could limit the mobility of OH groups that are instrumental in the sintering of HA and be the origin of the observed general lower sinterability of Si-HA. The favourable role of hydroxide vacancies on diffusion would be inhibited. Increasing the temperature to high enough values would then improve the mobility of OH, so that the behaviour of Si-HA matches that of HA with a deviation of ~100–150 °C. When densification occurs, the shrinkage rate seems to be higher for Si-HA than for pure HA (Fig. 2) [23], which would confirm the hypothesis of Pulayev et al. [35].

Finally, Si-HA appears as more refractory compounds than pure HA, which agrees with the behaviour of other silicate apatites such as $La_{9.33}(SiO_4)_6O_2$ or $Ca_9Nd(PO_4)_5(SiO_4)F_2$, which require high sintering temperatures [128,129].

4. Consolidation of nanocrystalline apatites

The use of nanosized particles is a common strategy in structural ceramic processing. These particles are characterized by a great surface area, which would increase the driving force of sintering by higher surface free energy (Eq. (1)). Sintering at lower temperatures could be used [130–133]. Xu et al. [130] used nanoparticles ~12 nm in size that were densified up to near full density by SPS at 1100 °C for 3 min. The resulting ceramic was a biphasic mixture of HA and TCP with a grain size of ~0.5 μm. Similarly, Chaudhry et al. [131] obtained fully dense HA (containing traces of TCP) with average grain size 220 nm from nanorods (length 165 nm, diameter 39 nm) after SPS at 1050 °C for 3 min (Table 2).

The total surface free energy of a powder also depends on its surface energy γ_{sg} (Eq. (1)). Interestingly, in order to increase the driving force of sintering, Wang and Shaw [133] used the specificity of HA nanorod morphology (length ~50 nm, diameter~15 nm), the surface of which is composed mainly of {0 0 1} crystallographic planes of high surface energy (1.16–1.54 J m^{-2} against 1.1 J m^{-2} for {1 0 0} planes). This allowed for the sintering of dense ceramics with very fine grains ($G \approx 80$ nm) at only 900 °C (Table 2). But more generally, the individual effect of particle size on the sintering of CaP is impossible to characterize precisely from the literature data. It is included in the results presented in Subsection 2.1 (see Tables 1 and 2).

For some years, a new approach has been investigated using nanocrystalline apatite particles analogous to bone mineral that can be synthesized by wet precipitation under so-called "bioinspired" conditions [134–136]. These have very high specific surface area and a low crystallinity associated with the presence of a hydrated surface layer, which contains highly mobile non-apatitic ions [134]. Enhanced bioreactivity and a major role in biomineralization are expected because of these properties. It would therefore be interesting to produce ceramic parts that would preserve these properties. But, whatever the sintering technique may be, in most studies the temperatures used were high enough to transform the initial particles to anhydrous and well-crystallized grains [137,138]. Novel innovative techniques of flash sintering, such as SPS, appear very promising in order to consolidate nanostructured

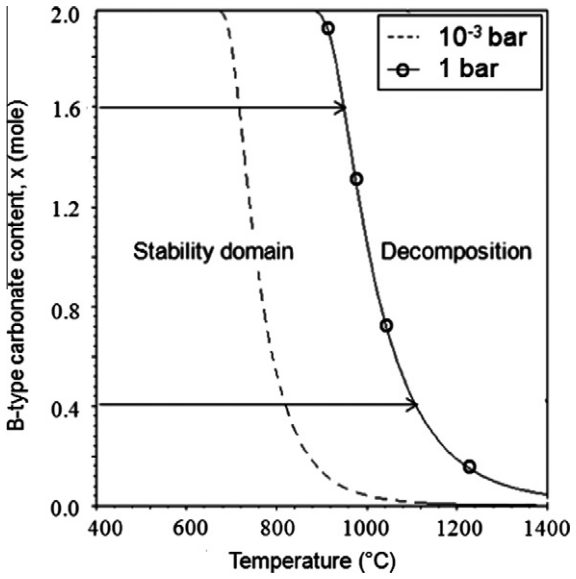

Fig. 8. Calculated isobaric curves of decarbonation equilibrium of B-type CO_3-HA in CO_2 atmosphere, after Ref. [119].

ceramics at very low temperatures ($T \leqslant 200$ °C) under high compressive stress ($P > 100$ MPa) without total degradation of the initial properties of biomimetic nanoparticles [139,140]. Under such unusual temperature conditions, solid-state matter mobility, which is classically involved in the sintering, is unlikely to occur. Though the mechanism inducing consolidation remains unclear, the mobility of ions within the surface hydrated layer of nanoparticles should play an important role. In addition to the driving force due to the pressing stress and to the presence of a great number of structural defects in such nanocrystals, this surface layer could act as a secondary liquid phase favouring diffusion.

5. Sintering of β-TCP

The sintering of TCP is much less reported than it is for HA. α-TCP and β-TCP are the two crystalline varieties of interest in biological applications. β-TCP is the thermodynamically stable form at low temperature. It transforms into α-TCP in the temperature range 1120–1170 °C [141,142]. β-TCP is generally preferred in sintered ceramic implants, while α-TCP is more commonly used in bone graft cements because of its hydrolysis properties [143]. TCP powder can be synthesized by aqueous precipitation of a CaDHA $Ca_{10-x}(PO_4)_{6-x}(HPO_4)_x(OH)_{2-x}$ with $x = 1$ (i.e. $Ca_9(PO_4)_5(HPO_4)(OH)$—apatitic tricalcium phosphate) [144–148]. Then, β-TCP can be obtained after calcination at $T > 700$ °C, which induces internal condensation of hydrogenphosphate groups according to the following reaction [20]:

$$Ca_{10-x}(PO_4)_{6-x}(HPO_4)_x(OH)_{2-x} \rightarrow (1-x)Ca_{10}(PO_4)_6(OH)_2 + 3xCa_3(PO_4)_2 + xH_2O_{(gas)} \quad (\text{with } x = 1) \qquad \text{(Reaction 8)}$$

Spray-pyrolysis [149] as well as solid-state reactions at high temperatures between biphasic mixtures of HA and $CaHPO_4$ [150,151], HA and a sulfate precursor [152], $CaHPO_4$ and $CaCO_3$ or $Ca_2P_2O_7$ and $CaCO_3$ [142,153] have also been used to produce β-TCP directly by reaction sintering. As detailed in Subsection 2.1.1, when CaDHA is used, superficial diffusion at low temperature may be detrimental to the sintering. In this case, a high heating rate in the intermediate temperature domain (from 400 up to 800 °C) in order to reduce grain coalescence or a precalcination above 700 °C to decompose the initial apatitic tricalcium phosphate intoβ-TCP followed by powder grinding to increase powder surface area can be applied to favour further densification.

The main difficulty encountered in the sintering of β-TCP comes from the β → α phase transformation that occurs at ~1150 °C. It is accompanied by a sudden dilatometric expansion (Fig. 1), which creates mechanical stresses inducing cracks within the sample [149,153]. This leads to a low mechanical reliability of TCP ceramics sintered above the transformation temperature [74]. Another point is that the reverse transformation α → β during cooling to room temperature does not occur in the same conditions as the β → α transformation, α-TCP being generally present in the cooled ceramics heated above the transformation temperature. Slow kinetics of the α → β transformation is often encountered in dimetallic phosphate compounds $Me_2(PO_4)_3$ [154]. According to the work of Monma and Goto [142], an annealing treatment of TCP for at least 5 h at 850 °C would be necessary to complete this transformation. To overcome these difficulties, some authors used MgO [99,151], ZnO [99,107,155], MgO–ZnO [156], MgO–SrO [157], SiO_2–ZnO [158] or $Ca_2P_2O_7$ [153] additives to increase the high-temperature limit of β-TCP. Similarly, the influence of TiO_2, Ag_2O, NaF, CaOor SiO_2 addition on the sintering of β-TCP has also been reported [107,148,159,160]. All these additives were also chosen because they were expected to improve the biological and/or mechanical properties of sintered ceramics.

Table 4 and Fig. 10 display the literature data on sintered β-TCP ceramics. As stated above, impurities may greatly change the temperature at which the β to α phase transformation occurs. Information about this purity should be provided, which is not the case in most of the studies presented in Table 4. Only the Ca/P ratio or the crystalline phases identified by X-ray diffraction (XRD) are given. So, the so-called "pure" TCP used hereafter refers to the observed crystalline phase and not to the chemical composition. Pressureless sintering of pure TCP appears somewhat similar to that of HA (Fig. 1). Densification begins at $T_B \approx 750$ °C and the sintering rate is maximum at a T_M of ~950–1000 °C (Fig. 2), a temperature which is slightly lower than that for HA ($T_M \approx 1050$ °C) [145,146,148]. The sintering trajectories (Fig. 10) indicate that, as for HA, grain growth occurs mainly during the last stage of sintering from ~95% of relative density. Though it is often stated that β-TCP is difficult to sinter without the β → α phase transformation, literature data (Table 4) show that nearly fully dense β-TCP can be produced at a temperature as low as 1100 °C without excessive

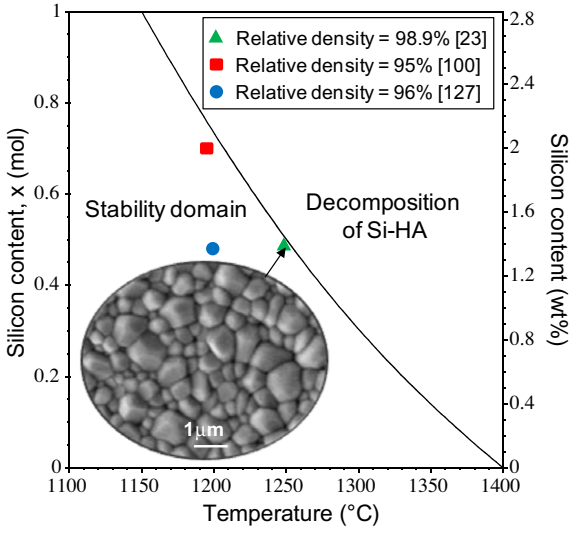

Fig. 9. Experimental decomposition curve of Si-HA in air (after Ref. [23]) and experimental literature data.

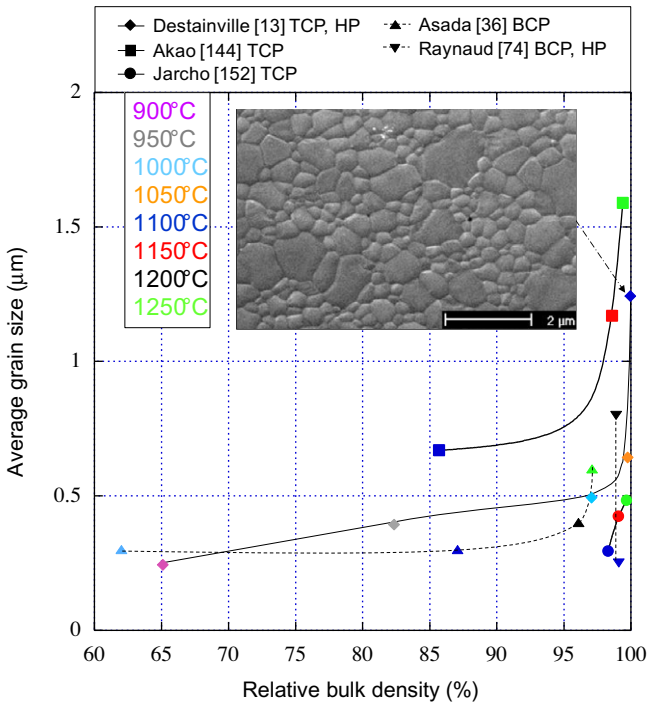

Fig. 10. Sintering trajectories of TCP and BCP.

grain growth (e.g. average grain size $G \approx 1$–2 µm; Fig. 11a). HP [13,150] and SPS [147] of pure TCP have also been investigated with the aim of fully densifying pure β-TCP at a temperature below the phase transformation. The results are summarized in Table 4. Tampieri et al. [150] used reaction sintering between HA and $CaHPO_4$ powder mixture. After HP at 1150 °C (1 h, 30 MPa) dense β-TCP containing ~10% of unreacted HA was obtained. Phase pure β-TCP was produced from CaDHA powders at 1050 °C [13] and 880 °C [147]. Because they require lower temperatures, these assisted sintering techniques (HP and more particularly SPS) allow this grain growth to be limited and hence produce β-TCP ceramics with grains of submicrometre size (Table 4) [13,147].

The use of additives to stabilize β-TCP up to higher temperature does not lead to better results, so they do not appear necessary to this purpose. Moreover, they generally lead to polyphasic ceramic materials in which phase composition and proportions are poorly controlled. Similarly, stoichiometry variations lead to impure TCP that may contain either HA (Ca/P > 1.50) or calcium pyrophosphate $Ca_2P_2O_7$ (Ca/P < 1.50) after sintering [22,145]. These impurities also influence the sintering behaviour, the sinterability increasing with the Ca/P ratio [22,146,161]. Though the presence of HA has only little influence, $Ca_2P_2O_7$ reduces the densification and induces fast and abnormal grain growth [22,146].

6. BCP ceramics

BCP ceramics made of a mixture of HA and β-TCP have been investigated as bone substitute materials for ~20 years, leading to commercially available products of various HA/TCP phase ratios [162]. These ceramics are usually produced from the sintering of HA/TCP powder mixtures or from a single phase CaDHA powder that thermally decomposes into the biphasic mixture according to Reaction (8). In this last case and as for apatitic TCP, superficial diffusion at low temperature must be prevented.

At higher temperatures ($T > 800$ °C) densification of a biphasic compact proceeds. The sintering ability of BCP is much lower than that of pure HA or β-TCP. An example of sintering trajectory is given in Fig. 10. As no evidence exists for any mutual sintering of HA and TCP, such materials can be seen as biphasic composites in which the minor phase acts as inert inclusions embedded in a matrix of the major phase. As mentioned previously, inclusions act as inhibitors of matrix sintering [73]. Consequently, high temperatures are required to produce nearly fully dense BCP ceramics by pressureless sintering. Temperatures of at least 1250 °C are commonly used [36,163–169]. These temperatures are superior to that of the β to α-TCP phase transformation. To overcome this problem, magnesium was added to stabilize β-TCP up to higher temperatures and allow sintering of BCP ceramics at 1300 °C without formation of α-TCP [170]. Alternatively, in agreement with the work of Monma and Goto [142] an annealing dwell at 900 °C for 24 h during cooling after sintering >1250 °C can be used to complete the reverse α-TCP to β-TCP transformation [169]. Assisted sintering such as HP [74,171] or TSS [172] can also be efficient at fully densifying β-TCP below the temperature of phase transformation (Fig. 10, Table 4). Moreover, grain growth can be limited using these last techniques (see the example in Fig. 11b and c [171]). Though the chemical reactions that occur during the formation of BCP from CadHA have been well described in Ref. [20], the morphological aspects are missing. It was shown using selective area electron diffraction (SAED) [171] that BCP ceramics resulted in a mixture of HA and TCP grains, TCP grains being slightly coarser (~0.5 µm) than HA grains (~0.1 µm) (Fig. 11), but the way they form and grow has not yet been elucidated.

Another approach in BCP processing is to sinter at low temperatures ($T \leqslant 1100$ °C) by either conventional sintering [162,164,173–175] or MWS [167,175,176]. In such cases, microporous ceramics are obtained. This corresponds to a recent trend in order to develop micro- and macroporous CaP ceramics with superior biological properties, micropores being expected to induce bone formation (e.g. osseoinduction) [177–180]. In this approach, the sintering is not completed and, owing to the resulting porosity, the mechanical reliability is generally low [181]. The use of specific shaping processes, such as hetero-coagulation with pore-forming polymeric microspheres [182,183] could be helpful for controlling pore size and porosity. This could also constitute an interesting alternative to incomplete sintering.

7. Microstructural design of sintered CaP ceramics

The microstructural design of sintered CaP ceramics includes numerous physical and chemical components: grain size, grain shape, grain orientation, porosity ratio, pore size, chemical composition of grains and grain boundaries, and surface charge. According to the sintering maps (Figs. 6, 7 and 10) the range of microstructures that can be offered by sintering appears somewhat restricted. Microstructures are generally made of equiaxed grains (see examples in Figs. 5 and 9–11), whose size may vary from a minimum of ~100 nm for nearly dense materials. A monomodal grain size distribution associated with normal grain growth is observed [23,74,148]. Only "prolonged" sintering may induce abnormal growth with bi- or multimodal grain size distributions (see inset in Fig. 10, for example). So, it could be stated from the sintering maps that CaP are not difficult to sinter. But, the final microstructural design of ceramics also depends on the chemical composition and physical properties of powders, and on the characteristics of the shaped body before sintering. Moreover, the development of new systems, such as nanostructured ceramics or multi-materials raises new issues.

7.1. Influence of chemical composition

The chemical composition of CaP is a crucial parameter, because a great number of ions can enter their crystal structure. These ions can be voluntarily incorporated during the synthesis of powders or

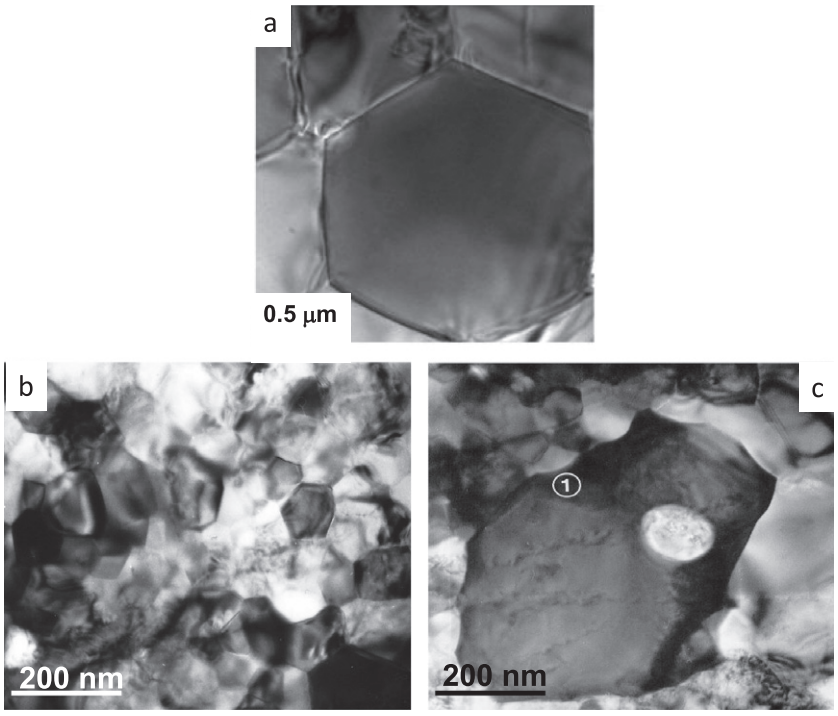

Fig. 11. (a) Typical hexagonal grain with flat boundaries (TCP, pressureless sintering, 1200 °C, 2 h) [40]. (b) Microstructure of fully dense BCP (88% HA–12% β-TCP hot pressed, 1100 °C, 20 MPa, 30 min) [171].

can be due to impurities. Dopants can also be mixed with CaP powders. The thermal stability of such systems as well as the chemical reactions that could occur may greatly change the sintering behaviour and, consequently, the final microstructural design of ceramics.

It was shown using Rietveld analysis that, during the sintering of a CaDHA, the HA phase formed from the thermal decomposition of the CaDHA (Reaction (8)) remained non-stoichiometric, even after 12 h at 1200 °C [184]. Thus, the relative proportions of HA and TCP phases present within the samples and their actual composition could vary, depending on the sintering temperature. This could be of interest for the development of novel multi-phasic ceramics, provided the chemical changes are mastered. More generally, particular behaviour can be expected during the sintering of multiphasic or multilayer materials. Such systems could be seen as composite materials. If there is no (or too low a rate) mutual (inter-) diffusion between the two phases, one can only expect the formation of a more or less chemically strong interface between grains or layers. This seems to be the case for BCP made of HA and TCP. If there is mutual diffusion between the two phases, the final product differs from the initial blend. In this field, the works of Gross et al. [44,122] on hydroxyfluorapatites showed that it is possible to change the chemical composition by solid-state diffusion from a biphasic hydroxyapatite and fluorapatite mixture into a solid solution hydroxyfluorapatite. Such an approach would be particularly valuable for the development of chemically graded or multilayered CaP ceramics that could be shaped from various techniques, such as tape casting, coatings or 3-D (ink jet) printing. Particular surface features can also be produced from reaction sintering of coated CaP substrate. For example, Nair et al. [185] sintered HA substrates coated with a silica sol at 1200 °C, which resulted in a triphasic outer surface layer containing HA, TCP and $CaSiO_4$. Similarly, surface charge can also be changed by the use of dopants [101].

Multiphasic systems also point to the importance of interfaces and/or grain boundaries. Surprisingly, this feature of the microstructure is seldom reported in the literature, though it can greatly influence the final properties of CaP ceramics. The thermal decomposition of substituted CaP or the reaction with additives or dopants can form amorphous phases or films, or crystalline particles segregated along the grain boundaries. As these phases may be present in very low amounts, structural analyses using transmission electron microscopy (TEM) and/or selective SAED coupled with energy dispersion spectroscopy (EDS) are required to determine their location and chemical nature. As mentioned in Section 2.1, no secondary phases, either crystalline or amorphous, formed along the grain boundary after sintering of pure HA at 1250 °C [25]. Only one study demonstrated from TEM that phase pure silicon substituted HA, i.e. without any intergranular phase, containing up to 2 wt.% of silicon could be produced after sintering at 1200 °C for 4 h [100]. It was also shown using SAED and EDS that silicon could hardly enter the β-TCP lattice and that it forms an amorphous silicon-rich phase [148]. In most studies, only XRD patterns are used to analyse the chemical composition, which is insufficient to state the real microstructural design of doped or substituted CaP.

7.2. Physical properties of powders and characteristics of shaped body

According to Tables 1, 3 and 4, the size, surface area, morphology of initial powders as well as the green density of samples may vary in a wide range. All these parameters may influence the sintering ability of CaP.

Various particle morphologies and sizes, from nanospheres or nanorods to spherical or fibrous micronic crystals, can be produced [138]. In most cases, powders are synthesized using the wet precipitation method (Tables 1, 3 and 4), which generally leads to nanorods with a high specific surface area, typically >50 $m^2 g^{-1}$ (Tables 1 and 3).

These powders can be sintered without any preparation before shaping green compacts (usually produced using uniaxial die pressing or cold isostatic pressing; Tables 1, 3 and 4). It was clearly

shown in several works that, during heating, rod-shaped HA nanoparticles grow from ~700 °C [133] and become equiaxed at 900 °C [44,133]. A similar result was found after SPS of HA powders at 825 °C for 3 min or 950 °C for 1 min under a uniaxial compressive stress of 50 MPa [92]. Only SPS at very high temperatures (1200 °C) for a long time (10 min) allowed the production of microstructures made of coarse elongated grains of HA with a length (*c*-axis of crystals) >50 μm [91,94]. Such particular textured microstructure resulted from an important grain growth that occurred during this "prolonged" sintering. Thus, very low temperatures should be used to preserve the morphology of initial particles and develop microstructures made of nanosized (needle-like) grains. Moreover, a texturation effect can be obtained using an additional applied uniaxial stress (SPS). Indeed, it can induce a preferred orientation of elongated particles (in the *c*-axis direction of crystals), which tend to lie in planes perpendicular to the direction of the applied stress [140].

Several treatments, including washing, drying, calcination, grinding, addition of binders (such as polyvinyl alcohol PVA [11,79,147] or polyvinyl butyral PVB [24]) or granulation by spray drying [15,75] (Tables 1, 3 and 4) can be performed before shaping and further sintering. Washing with distilled water or ethanol is used to remove the by-products contained in the powders synthesized by the wet methods. Such a treatment should not significantly alter the solid particles, and there is no clear evidence in the literature for any direct influence of powder washing on the further sintering ability. Nevertheless, because of the low solubility of CaP, a very small decrease in the particle size could occur during washing. The most significant effect is a modification of particles' surface charge, which depends on the nature of the solvent. The low dielectric constant and surface tension of alcohol induce a very low ionic strength of the solution and an enhanced wettability of particles, which results in loosely bonded particles [44]. Thus, washing with ethanol should be more favourable than with water for further deagglomeration of particles. Similarly, freeze-drying of powders after washing can be preferred to conventional heat-drying, which leads to a strong agglomeration [186,187]. Deagglomerated particles and a high surface area are favourable, and it is well known that, for enhanced sintering rates and the attainment of high density, the particles must be homogeneously packed with high packing density [17]. The influence of the green density and powder surface area on the sintering rate of CaP has been reported in several works [21,86,132,138,188]. In order to adapt the powders' properties to the shaping processes, a calcination treatment is often performed before sintering. It induces grain growth and surface area reduction. Further grinding after calcination to break particle agglomerates or aggregates is necessary. For the same reason as during washing, ethanol can be preferred to water as a liquid medium during the grinding or ball milling of the powder [14,24,44,153]. Some shaping processes, such as tape casting or rapid prototyping (3-Dprinting, stereolithography), require slurries containing a high volume fraction of polymeric binders, which may also reduce the packing density of ceramic particles and consequently the sinterability.

Finally, the main difficulties come from the development of new objects and microstructures and, more particularly, in the case of nanostructured and/or multi-phasic materials. Nanometric particles are generally highly agglomerated, which is not favourable to homogeneous and high-density packing. This difficulty is increased with rod-shaped particles. Moreover, they are generally metastable with a high thermal reactivity. Because of grain growth during sintering, nanoceramics (i.e. with grain size <100 nm) can only be produced by flash sintering or consolidation at very low temperatures. In this field, new approaches, including various shaping methods (as those mentioned earlier) before sintering should help to provide new geometries as well as micro/nano-structural designs.

8. Summary and concluding remarks

The sintering of hydroxyapatite ceramics has been widely studied for about 40 years. The parameters involved in the densification and grain growth have been identified. The hydroxyl column, which may contain hydroxide ions, vacancies or substituted ions, plays an important role. Through the advancement of the dehydroxylation reaction, lattice vacancies enhance both grain coalescence in the first stage of sintering at low temperatures and densification during the intermediate stage at higher temperatures. During the final stage, when pores are closed, dehydroxylation can also inhibit densification because of trapped water vapour. Substituted ions may change interaction forces within the lattice that change the ions' mobility and the sintering ability. But, whatever the composition of CaP may be, the transition point between the phenomena promoting densification to those favouring grain growth occurs at ~95% of relative bulk density.

Grain growth occurs simultaneously to the densification process. But it is particularly active during the last stage of sintering and promoted by high temperatures. Densification techniques other than conventional solid-state pressureless sintering, such as HP, HIP, MWS, SPS or TSS, have been investigated for producing CaP ceramics with fine grains. Similarly, numerous sintering aids were studied. Enhancement of the mechanical reliability could be expected from these approaches, but it still appears insufficient and, as reviewed by Wagoner Johnson and Herschler [8], the very low toughness of CPC still remains critical for load-bearing applications. Moreover, these mechanical properties will degrade to a significant extent after implantation, as was shown after soaking in liquid medium [181,189]. This relates directly to the bioactivity of CPC, which is induced by their solubility in body fluids and resorbability through osteoclast activity. From this point of view, simultaneously improving the mechanical and biological properties could even appear contradictory. Finally, optimized pressureless sintering (in a controlled atmosphere when necessary) remains the most useful and the reference technique for producing dense CPC with a fine microstructure. Nevertheless, alternative sintering methods have not been investigated as much as conventional sintering. Their optimization should lead to further improvements. This is particularly the case for TSS and flash sintering techniques or low-temperature consolidation, which should be helpful for producing ceramics with a controlled nanoscale grain size or with nanostructured microstructures.

Numerous works aiming to improve biological behaviour have been devoted to the addition of second phases or of substituted ions in HA, TCP or BCP. In many studies, the final composition of ceramics after sintering is for the most part uncontrolled (exact nature, proportions and distribution of chemical species and phases). Some authors even use the term "HA" to describe other chemical compounds. As recently exposed in the case of silicon [190], one must be cautious with regard to the conclusions that state-enhanced biological properties due to a particular substituted chemical element or doping chemical compound, because its location and the whole microstructural design of the sintered ceramic is rarely characterized accurately. Important microstructural changes may be induced (presence of either amorphous or crystalline second phases, intergranular phases, grain boundaries of various thickness and composition), which should also contribute to the biological behaviour.

Currently, new trends have arisen in the field of CPC. They are mainly oriented towards superior biological properties through the development of multiscale micro–macroporous architectures with complex shapes, multi-materials combining various CaP, composites, hybrid materials or biomimetic nanopatite ceramics. To this end, very low temperature consolidation using innovative

techniques such as SPS or other electric current activated sintering seems of particular interest. Though this paper focused on sintering, the powder preparation and shaping processes are also of crucial importance for the development of reliable CPC with controlled architecture and chemical composition.

Appendix. Figures with essential color discrimination

Certain figures in this article, particularly Figs. 1, 2, 6, 7, 9 and 10, are difficult to interpret in black and white. The full colour images can be found in the on-line version, at doi http://dx.doi.org/10.1016/j.actbio.2012.11.029.

References

[1] Hench LL. Bioceramics. J Am Ceram Soc 1998;81:1705–28.
[2] Hench LL, Polak JM. Third-generation biomedical materials. Science 2002;295:1014–7.
[3] Jarcho M. Calcium phosphate ceramics as hard tissue prosthetics. Clin Orthop Rel Res 1981;157:259–78.
[4] De Groot K. Bioceramics of calcium phosphate. Boca Raton, Fl: CRC Press; 1983.
[5] Ravaglioli A, Krajewski A. In: Bioceramics. London: Chapman & Hall; 1992. p. 254.
[6] Albee FH. Studies in bone growth triple calcium phosphate as a stimulus to osteogenesis. Ann Surg 1920;71:32.
[7] Monroe EA, Votava W, Bass DB, McMullen J. New calcium phosphate ceramic material for bone and tooth implants. J Dental Res 1971;50:860–1.
[8] Wagoner Johnson AJ, Herschler BA. A review of the mechanical behavior of CaP and CaP/polymer composites for applications in bone replacement and repair. Acta Biomater 2011;7:16–30.
[9] Jarcho M, Bolen CH, Thomas MB, Bobick J, Kay JF, Doremus RH. Hydroxylapatite synthesis and characterization in dense polycrystalline form. J Mat Sci 1976;11:2027–35.
[10] De With G, Van Dijk HJA, Hattu N, Prijs K. Preparation, microstructure and mechanical properties of dense polycrystalline hydroxyapatite. J Mat Sci 1981;16:1592–8.
[11] Akao M, Miura N, Aoki H. Fracture toughness of sintered hydroxyapatite and β-tricalcium phosphate. Yogyo Kyoka-Shi 1984;92:672–4.
[12] Halouani R, Bernache-Assollant D, Champion E, Ababou A. Microstructure and related mechanical properties of hot pressed hydroxyapatite ceramics. J Mat Sci Mater Med 1994;5:563–8.
[13] Destainville A, Rolo A, Champion E, Bernache-Assollant D. Synthesis and characterization of beta tricalcium phosphate. Key Eng Mat 2003;240–242:489–92.
[14] Laasri SZ, Taha M, Laghzizil, Hlil EK, Chevalier J. The affect of densification and dehydroxylation on the mechanical properties of stoichimetric hydroxyapatite bioceramics. Mat Res Bul 2010;45:1433–7.
[15] Royer A, Viguie JC, Heughebaert M, Heughebaert JC. Stoichiometry of hydroxyapatite: influence on the flexural strength. J Mat Sci Mater Med 1993;4:76–82.
[16] Kuczynski GC. Physics and chemistry of sintering. Adv Coll Int Sci 1972;3:275–330.
[17] Rahaman MN. Sintering of ceramics. Boca Raton: CRC Press; 2008.
[18] Bernache-Assollant D. Chimie-physique du frittage (Physico-chemistry of sintering). Paris: Hermes; 1993.
[19] Landi E, Tampieri A, Celotti G, Sprio S. Densification behaviour and mechanisms of synthetic hydroxyapatites. J Eur Ceram Soc 2000;20:2377–87.
[20] Mortier A, Lemaitre J, Rouxhet PG. Temperature-programmed characterization of synthetic calcium-deficient phosphate apatites. Thermochimica Acta 1989;143:265–82.
[21] Pramanik S, Agarwal AK, Rai KN, Garg A. Development of high strength hydroxyapatite by solid-state-sintering process. Ceram Int 2007;33:419–26.
[22] Raynaud S, Champion E. Bernache assollant. Calcium phosphate apatites with variable Ca/P atomic ratio II. Calcination and sintering. Biomaterials 2002;23:1073–80.
[23] Palard M, Combes J, Champion E, Foucaud S, Rattner A, Bernache-Assollant D. Effect of silicon content on the sintering and biological behaviour of $Ca_{10}(PO_4)_{6-x}(SiO_4)_x(OH)_{2-x}$ ceramics. Acta Biomater 2009;5:1223–32.
[24] Fateeva LV, Golovkov YI, Tumanov SV, Barinov SM, Shemyakina AN, Orlovskii VP, et al. Effect of sodium phosphate on sintering of hydroxyapatite ceramics. Refract Ind Ceram 2001;42:3–8.
[25] Kleebe HJ, Bres EF, Bernache-Assollant D, Ziegler G. High-resolution electron microscopy and convergent beam electron diffraction of sintered undoped hydroxyapatite. J Am Ceram Soc 1997;80:37–44.
[26] Zhou J, Zhang X, Chen J, Zeng S, De Groot K. High temperature characteristics of synthetic hydroxyapatite. J Mat Sci Mater Med 1993;4:83–5.
[27] Raynaud S, Champion E, Bernache Assollant D, Thomas P. Calcium phosphate apatites with variable Ca/P atomic ratio I. Synthesis, characterisation and thermal stability of powders. Biomaterials 2002;23:1065–72.
[28] Liao CJ, Lin FH, Chen KS, Sun JS. Thermal decomposition and reconstruction of hydroxyapatite in air atmosphere. Biomaterials 1999;20:1807–13.
[29] Riboud PV. Composition et stabilité des phases à structure d'apatite dans le système $CaO–P_2O_5$–Oxyde de fer–H_2O à haute température. Ann Chim Fr 1973;8:381–90.
[30] Kijima T, Tsutsumi M. Preparation and thermal properties of dense polycrystalline oxyhydroxyapatite. J Am Ceram Soc 1979;63:455–60.
[31] Palard M. Synthèse, frittage et évaluation biologique d'hydroxyapatites silicatées (Synthesis, sintering and biological evaluation of silicated hydroxyapatites). PhD thesis. France: University of Limoges; 2007.
[32] Rootare HM, Craig RG. Characterization of the compaction and sintering of hydroxyapatite powders by mercury porosimetry. Powder Tech 1974;9:199–211.
[33] Bernache-Assollant D, Ababou A, Champion E, Heughebaert M. Sintering of calcium phosphate hydroxyapatite $Ca_{10}(PO_4)_6(OH)_2$ I. Calcination and particle growth. J Eur Ceram Soc 2003;23:229–41.
[34] Pask JA. Effect of water vapor on sintering of ceramic oxides. In: Somiya S, editor. Proceedings 1st international symposium on hydrothermal reactions. Tokyo: Tokyo Institute of Technology; 1983. p. 904–18.
[35] Putlayev V, Veresov A, Pulkin M, Soin A, Kuznetsov V. Silicon-substituted hydroxyapatite ceramics (Si-Hap): densification and grain growth through the prism of sintering theories. Mat wiss u werkstofftech 2006;37:416–21.
[36] Asada M, Oukami K, Nakamura S, Takahashi K. Microstructure and mechanical properties on non-stoichiometric apatite ceramics and sinterability of raw powder. J Ceram Soc Jpn Int Ed 1988;96:583–6.
[37] Lukic MJ, Veselinovic L, Stojanovic Z, Macek-Krzmanc M, Bracko I, Skapin SD, et al. Particularities in sintering behavior of Ca-deficient hydroxyapatite nanopowders. Mat Let 2012;68:331–5.
[38] Rootare HM, Craig RG. Characterization of hydroxyapatite powders and compacts at room temperature and after sintering at 1200 °C. J Oral Rehab 1978;5:293–307.
[39] Brook RJ. Controlled grain growth. In: Wang FY, editor. Treatise on materials science and technology. New York: Academic Press; 1976. p. 331–64.
[40] Douard N. Elaboration et fonctionnalisation de biocéramiques phosphocalciques (Processing and functionalization of calcium phosphate bioceramics). PhD thesis. France: University of Limoges; 2010.
[41] Akao M, Aoki H, Kato K. Mechanical properties of sintered hydoxyapatite for prosthetic applications. J Mat Sci 1981;16:809–12.
[42] He LH, Standard OC, Huang TTY, Latella BA, Swain MS. Mechanical behaviour of porous hydroxyapatite. Acta Biomater 2008;4:577–86.
[43] Lin FH, Harn TL, Hon MH. A study on synthesized hydroxylapatite bioceramics. Ceram Int 1989;15:351–6.
[44] Gross KA, Rodriguez-Lorenzo LM. Sintered hydroxyfluorapatites. Part I: sintering ability of precipitated solid solution powders. Biomaterials 2004;25:1375–84.
[45] Ramesh S, Tan CY, Bhaduri SB, Teng WD, Sopyan I. Densification behavior of nanocrystalline hydroxyapatite bioceramics. J Mat Proc Tech 2008;206:221–30.
[46] Mazaheri M, Haghighatzadeh M, Zahedi AM, Sadrnezhaad SK. Effect of a novel sintering process on mechanical properties of hydroxyapatite ceramics. J Alloys Compd 2009;471:180–4.
[47] Fanovich MA, Porto-Lopez JM. Influence of temperature and additives on the microstructure and sintering behavior of hydroxyapatites with different Ca/P ratios. J Mat Sci Mater Med 1998;9:53–60.
[48] Barralet JE, Fleming GJP, Campion C, Harris JJ, Wright AJ. Formation of translucent hydroxyapatite ceramics by sintering in carbon dioxide atmospheres. J Mat Sci 2003;38:3979–93.
[49] Liu Y, Shen Z. Dehydroxylation of hydroxyapatite in dense bulk ceramics sintered by spark plasma sintering. J Eur Ceram Soc 2012;32:2691–6.
[50] Van Landuyt P, Li F, Keustermans JP, Streydio JM, Delannay F. The influence of high sintering temperature on the mechanical properties of hydroxyapatite. J Mat Sci Mater Med 1995;6:8–13.
[51] Mullins W, Vinals J. Self-similarity and growth kinetics driven by surface free energy reduction. Acta Metall 1989;37:991–7.
[52] Chen PL, Chen IW. Role of defect interaction in boundary mobility and cation diffusivity of CeO_2. J Am Ceram Soc 1994;77:2289–97.
[53] Tetard F, Bernache-Assollant D, Champion E, Lortholary P. Grain growth kinetics of Li_3PO_4-doped calcium carbonate. Solid State Ionics 1997;101–103:517–25.
[54] Wang PE, Chaki TK. Sintering behavior and mechanical properties of hydroxyapatite and dicalcium phosphate. J Mat Sci Mater Med 1993;4:150–8.
[55] Tagai H, Aoki H. Preparation of synthetic hydroxyapatite and sintering of apatite ceramics. In: Hastings GW, Williams DF, editors. Mechanical properties of biomaterials. John Wiley & sons; 1980. p. 477–88.
[56] Peelen JGJ, Rejda B, De Groot K. Preparation and properties of sintered hydroxylapatite. Ceramurgia Int 1978;4:71–4.
[57] Lafon JP, Champion E, Bernache-Assollant D. Processing of AB-type carbonated hydroxyapatite $Ca_{10-x}(PO_4)_{6-x}(CO_3)_x(OH)_{2-x-2y}(CO_3)_y$ ceramics with controlled composition. J Eur Ceram Soc 2008;28:139–47.
[58] Seuter AMJH. Existence region of hydroxylapatite and the equilibrium with coexisting phases at elevated temperatures. In: Anderson JS, Robert MW, Stone FS, editors. Reactivity of solids. London: Chapman & Hall; 1972. p. 806–12.
[59] Bonel G. Contribution à l'étude dela carbonatation des apatites-1-Synthèse et étude des propriétés phisico-chimiques des apatites carbonatées de type A. Ann Chim Fr 1972;7:65–88.

[60] Chen IW, Wang XH. Sintering dense nanocrystalline ceramics without final-stage grain growth. Nature 2000;404:168–70.
[61] Kingery WD. Densification during sintering in the presence of a liquid phase. I. Theory. Appl Phys 1959;30:301–6.
[62] Marion JE, Hsueh CH, Evans AG. Liquid-phase sintering of ceramics. J Am Ceram Soc 1987;70:708–13.
[63] Kondo K, Okuyama M, Ogawa H, Shibata Y. Preparation of high strength apatite ceramics. Com Am Ceram Soc 1984;67:C-222–3.
[64] Santos JD, Reis RL, Monteiro FJ, Knowles JC, Hastings GW. Liquid phase sintering of hydroxyapatite by phosphate and silicate glass additions: structure and properties of the composites. J Mat Sci Mater Med 1995;6:348–52.
[65] Santos JD, Silva PL, Knowles JC, Talal S, Monteiro FJ. Reinforcement of hydroxyapatite by adding P_2O_5–CaO glasses with Na_2O, K_2O and MgO. J Mat Sci Mater Med 1996;7:187–9.
[66] Kangasniemi I, De Groot K, Wloke J, Andersson O, Luklinska Z, Becht JGM, et al. The stability of hydroxyapatite in an optimized bioactive glass matrix at sintering temperature. J Mat Sci Mater Med 1991;2:133–7.
[67] Georgiou G, Knowles JC, Barralet JE. Dynamic shrinkage behavior of hydroxyapatite and glass-reinforced hydroxyapatite. J Mat Sci 2004;39:2205–8.
[68] Kalita SJ, Bose S, Hosick HL. Bandyopadhyay. CaO–P_2O_5–Na_2O-based sintering additives for hydroxyapatite (Hap) ceramics. Biomaterials 2004;25:2331–9.
[69] Goto T, Wakamatsu N, Kamemizu H, Iijima M, Doi Y, Moriwaki Y. Sintering mechanism of hydroxyapatite by addition of lithium phosphate. J Mat Sci Mater Med 1991;2:149–52.
[70] Ababou A, Bernache-Assollant D. Sintering hydroxyapatite with differentadditives. In: Ravaglioli A, editor. Fourth Euro Ceramics – Bioceramics. Faenza: Gruppo Editoriale Faenza Editrice S.p.A; 1995. p. 185–90.
[71] Fanovich MA, Castro MS, Porto Lopez JM. Improvement of the microstructure and microhardness of hydroxyapatite ceramics by addition of lithium. Mat Lett 1998;33:269–72.
[72] Suchanek W, Yashima M, Kakihana M, Yoshimura M. Hydroxyapatite ceramics with selected sintering additives. Biomaterials 1997;18:923–33.
[73] Scherer GW. Sintering with rigid inclusions. J Am Ceram Soc 1987;70:719–25.
[74] Raynaud S, Champion E, Lafon JP, Bernache Assollant D. Calcium phosphate apatites with variable Ca/P atomic ratio III. Mechanical properties and degradation in solution of hot pressed ceramics. Biomaterials 2002;23:1081–9.
[75] Veljovic D, Jokic B, Petrovic R, Palcevskis E, Dindune A, Mihailescu IN, et al. Processing of dense nanostructured HAP ceramics by sintering and hot pressing. Ceram Int 2009;35:1407–13.
[76] Hirota K, Hasegawa YT, Monma H. Densification of hydroxyapatite by hot isostatic pressing. Yogyo-Kyokai-Shi 1982;90:62–4.
[77] Hirayama Y, Ikata H, Akiyama H, Naganuma K, Ojima S, kawakami M. Sintering characteristics and mechanical property of hydroxyapatite. In: Somiya S, Shimasa M, Yoshimura M, Watanabe M, editors. Sintering. London: Elsevier Applied Science; 1988. p. 1332–1337.
[78] Wakai F, Kodama Y, Sakaguchi S. Superplasticity of hot isostatically pressed hydroxyapatite. J Am Ceram Soc 1990;73:457–60.
[79] Takikawa K, Akao M. Fabrication of transparent hydroxyapatite and application to bone marrow derived cell/hydroxyapatite interaction observation in-vivo. J Mat Sci Mater Med 1996;7:439–45.
[80] Uematsu K, Takagi M, Honda T, Uchida N, Saito K. Transparent hydroxyapatite prepared by hot isostatic pressing of filter cake. J Am Ceram Soc 1989;72:1476–8.
[81] Li J, Hermansson L. Mechanical evaluation of hot isostatically pressed hydroxylapatite. Interceram 1990;39:13–5.
[82] Tan N, Kou Z, Ding Y, Leng Y, Liu C, He D. Novel substantial reductions in sintering temperatures for preparation of transparent hydroxyapatite bioceramics under ultrahigh pressure. Scripta Mater 2011;65:819–22.
[83] Agrawal KD. Microwave processing of ceramics. Curr Opin Solid State Mat Sci 1998;3:480–5.
[84] Oghbaei M, Mirzaee O. Microwave versus conventional sintering: a review of fundamentals, advantages and applications. J All Comp 2010;494:175–89.
[85] Fang Y, Agrawal DK, Roy DM, Roy R. Fabrication of porous hydroxyapatite ceramics by microwave processing. J Mater Res 1992;7:490–4.
[86] Fang Y, Agarwal DK, Roy DM, Roy R. Microwave sintering of hydroxyapatite ceramics. J Mater Sci 1994;9:180–7.
[87] Veljovik D, Zalite I, Palecvskis E, Smiciklas I, Petrovic R, Janackovic. Microwave sintering of fine grained HAP and HAP/TCP bioceramics. Ceram Int 2010;45:595–603.
[88] Chanda A, Dasgupta S, Bose S, Bandyopadhyay. Microwave sintering of calcium phosphate ceramics. Mat Sci Eng C 2009;29:1144–9.
[89] Orru R, Licheri R, Locci AM, Cincotti A, Cao G. Consolidation/synthesis of materials by electric current activated/assisted sintering. Mat Sci Eng R 2009;63:127–287.
[90] Gu YW, Loh NH, Khor KA, Tor SB, Cheang P. Spark plasma sintering of hydroxyapatite powders. Biomaterials 2002;23:37–43.
[91] Nakahira A, Tamai M, Eguchi K, Nakamura S, Yamashita K. Preparation and evaluation of dense hydroxyapatite by PECS method. Key Eng Mat 2003;240–242:551–4.
[92] Guo X, Xiao P, Liu J, Shen Z. Fabrication of nanostructured hydroxyapatite via hydrothermal synthesis and spark plasma sintering. J Am Ceram Soc 2005;88:1026–9.
[93] Eriksson M, Liu Y, Hu J, Gao L, Nygren M, Shen Z. Transparent hydroxyapatite ceramics with nanograin structure prepared by high pressure spark plasma sintering at the minimized sintering temperature. J Eur Ceram Soc 2011;31:1533–40.
[94] Watanabe Y, Ikoma T, Monkawa A, Suetsugu Y, Yamada H, Tanaka J, et al. Fabrication of transparent hydroxyapatite sintered body with high crystal orientation by pulse electric current sintering. J Am Ceram Soc 2005;88:243–5.
[95] Yu LG, Khor KA, Li H, Cheang P. Effect of spark plasma sintering on the microstructure and in vitro behavior of plasma sprayed HA coatings. Biomaterials 2003;24:2695–705.
[96] Rossignol F, Goursat P, Besson JL. Microstructure and mechanical behaviour of self-reinforced Si_3N_4 and Si_3N_4–SiC whisker composites. J Eur Ceram Soc 1994;13:299–312.
[97] Cacciotti I, Bianco A, Lombardi M, Montanaro L. Mg-substituted hydroxyapatite nanopowders: synthesis, thermal stability and sintering behaviour. J Eur Ceram Soc 2009;29:2969–78.
[98] Gibson IR, Bonfield W. Preparation and characterization of magnesium/carbonate co-substituted hydroxyapatites. J Mater Sic Mater Med 2002;13:685–93.
[99] Rabadjieva D, Tepavitcharova S, Gergulova R, Sezanova K, Titorenkova R, Petrov O, et al. Mg- and Zn-modified calcium phosphates prepared by biomimetic precipitation and subsequent treatment at high temperature. J Mater Sci Mater Med 2011;22:2187–96.
[100] Kim SR, Lee HJ, Kim YT, Riu DH, Jung SJ, Lee YJ, et al. Synthesis of Si, Mg substituted hydroxyapatites and their sintering behaviours. Biomaterials 2003;24:1389–98.
[101] Bodhak S, Bose S, Bandyopadhyay A. Influence of MgO, SrO and ZnO dopants on electro-thermal polarization behavior and in vitro biological properties of hydroxyapatite ceramics. J Am Ceram Soc 2011;94:1281–8.
[102] Kobune M, Mineshige A, Fujii S, Iida H. Preparation of translucent hydroxyapatite by HIP and their physical properties. J Ceram Soc Jpn 1997;105:210–3.
[103] Landi E, Tampieri A, Celotti G, Sprio S, Sandri M, Logroscino G. Sr-substituted hydroxyapatites for osteoporotic bone replacement. Acta Biomater 2007;3:961–9.
[104] Takeda H, Seki Y, Nakamura S, Yamashita K. Evaluation of electrical polarizability and in vitro bioactivity of apatite $Sr_5(PO_4)_3OH$ dense ceramics. J Mat Chem 2002;12:2490–5.
[105] Curran DJ, Fleming TJ, Towler MR, Hampshire S. Mechanical parameters of strontium doped hydroxyapatite sintered using microwave and conventional methods. J Mech Behav Biomed Mat 2011;4:2063–73.
[106] Xue W, Moore JL, Hosick HL, Bose S, Bandyopadhyay A, Lu WW, et al. Osteoprecursor cell response to strontium-containing hydroxyapatite ceramics. J Biomed Mater Res 2006;79A:804–14.
[107] Bandyopadhay A, Withney EA, Moore J, Bose S. Influence of ZnO doping in calcium phosphate ceramics. Mater Sci Eng C 2007;27:14–7.
[108] Ramesh S, Tan CY, Yeo WH, Tolouei R, Amiriyan M, Sopyan I, et al. Effects of bismuth oxide on the sinterability of hydroxyapatite. Ceram Int 2011;37:599–606.
[109] Kannan S, Venturer JMG, Ferreira JMF. Synthesis and thermal stability of potassium substituted hydroxyapatites and hydroxyapatite/β-tricalcium phosphate mixtures. Ceram Int 2007;33:1489–94.
[110] Nakahira A, Shiba K, Yamaguchi S, Kijima K. Effect of Y_2O_3 on sintering and microstructure of hydroxyapatite. Key Eng Mat 1999;161–163:177–80.
[111] Fadeev IV, Shvorneva LI, Barinov SM, Orlovskii VP. Synthesis and structure of magnesium-substituted hydroxyapatite. Inorg Mater 2003;9:947–50.
[112] Legeros RZ. Calcium phosphates in oral biology and medicine. In: Myers HM, editor. Monographs in oral science. Basel: Karger; 1991.
[113] Gibson IR, Bonfield W. Novel synthesis and characterization of an AB-type carbonate-substituted hydroxyapatite. J Biomed Mater Res 2002;59:697–708.
[114] Landi E, Tampieri A, Celotti G. Influence of synthesis and sintering parameters on the characteristics of carbonate apatite. Biomaterials 2004;25:1763–70.
[115] Lafon JP, Champion E, Bernache-Assollant D, Gibert R, Danna AM. Thermal decomposition of carbonated calcium phosphate apatites. J Therm Anal Calorim 2003;72:1127–34.
[116] Doi Y, Koda T, Wakamatsu N, Goto T, Kamemizu H, Moriwaki Y, et al. Influence of carbonate on sintering of apatites. J Dental Res 1993;9:1279–84.
[117] Barralet JE, Best SM, Bonfield W. Effect of sintering parameters on the density and microstructure of carbonate hydroxyapatite. J Mater Sci Mater Med 2000;11:719–24.
[118] Slosarczyk A, Paszkiewicz Z, Zima A. The effect of phosphate source on the sintering of carbonate substituted hydroxyapatite. Ceram Int 2010;36:577–82.
[119] Lafon JP. Champion E, Bernache Assollant D. Thermal behaviour of synthetic carbonate hydroxyapatite in various atmospheres: experimental approach and thermodynamical modelling, in preparation.
[120] Driessens FC, Veerbeck RMH, Kiekens P. Mechanism of substitution in carbonated apatites. Z Anorg Allg Chemie 1983;504:195–200.
[121] Senamaud N, Bernache-Assollant D, Champion E, Heughebaert M, Rey C. Calcination and sintering of hydroxyfluorapatite powders. Solid State Ionics 1997;101–103:1357–62.
[122] Gross KA, Bhadang KA. Sintered hydroxyfluorapatites. Part III: sintering and resultant mechanical properties of sintered blends of hydroxyapatite and fluorapatite. Biomaterials 2004;25:1395–405.

[123] Ben Ayed F, Bouaziz J, Bouzouita K. Calcination and sintering of fluorapatite under argon atmosphere. J Alloys Comp 2001;322:238–45.
[124] Gibson IR, Best SM, Bonfield W. Effect of silicon substitution on the sintering and microstructure of hydroxyapatite. J Am Ceram Soc 2002;85:2771–7.
[125] Bianco A, Cacciotti I, Lombardi M, Montanaro L. Si-substituted hydroxyapatite nanopowders: synthesis, thermal stability and sinterability. Mater Res Bull 2009;44:345–54.
[126] Ruys AJ. A feasibility study of silicon doping of hydroxylapatite. Interceram 1993;42:372–4.
[127] Porter AE, Patel N, Skepper JN, Best SM, Bonfield W. Comparison of in vivo dissolution processes in hydroxyapatite and silicon-substituted hydroxyapatite bioceramics. Biomaterials 2003;24:4609–20.
[128] Bechade E, Julien I, Iwata T, Masson O, Thomas P, Champion E, et al. Synthesis of lanthanum silicate oxyapatite materials for solid oxide fuel cells electrolyte. J Eur Ceram Soc 2008;28:2717–24.
[129] Brégiroux D, Audubert F, Champion E, Bernache-Assollant D. Mechanical and thermal properties of hot pressed neodymium-substituted britholite $Ca_9Nd(PO_4)_5(SiO_4)F_2$. Mater Lett 2003;57:3526–31.
[130] Xu JL, Khor KA, Kumar R. Physicochemical differences after densifying radiofrequency plasma sprayed hydroxyapatite powders using spark plasma and conventional sintering techniques. Mater Sci Eng A 2007;457:24–32.
[131] Chaudhry AA, Yan H, Gong K, Inam F, Viola G, Reece MJ, et al. High-strength nanograined and translucent hydroxyapatite monoliths via continuous hydrothermal synthesis and optimized spark plasma sintering. Acta Biomater 2011;7:791–9.
[132] Gibson IR, Ke S, Best SM, Bonfield W. Effect of powder characteristics on the sinterability of hydroxyapatite powders. J Mater Sci Mater Med 2001;12:163–71.
[133] Wang J, Shaw LL. Morphology-enhanced low-temperature sintering of nanocrystalline hydroxyapatite. Adv Mater 2007;19:2364–9.
[134] Eichert D, Drouet C, Sfihi H, Rey C, Combes C. Nanocrystalline apatite-based biomaterials: synthesis, processing and characterisation. In: Kendall BJ, editor. Biomaterials research advances. Hauppauge, NY: Nova Science Publishers; 2007. p. 93–143.
[135] Dorozhkin SV. Nanosized and nanocrystalline calcium orthophosphates. Acta Biomater 2010;6:715–34.
[136] Kalita SJ, Bhardwaj A, Bhatt HA. Nanocrystalline calcium phosphate ceramics in biomedical engineering. Mater Sci Eng C 2007;27:441–9.
[137] Zhang F, Lin K, Chang J, Lu J, Ning C. Spark plasma sintering of macroporous calcium phosphate scaffolds from nanocrystalline powders. J Eur Ceram Soc 2008;28:539–45.
[138] Hong Y, Fan H, Li B, Guo B, Liu M, Zhang X. Fabrication, biological effects, and medical applications of calcium phosphate nanoceramics. Mater Sci Eng R 2010;70:225–42.
[139] Drouet C, Largeot C, Raimbeaux G, Estournès C, Dechambre G, Combes C, et al. Bioceramics: spark plasma sintering (SPS) of calcium phosphates. Adv Sci Tech 2006;49:45–50.
[140] Grossin D, Rollin-Martinet S, Estournes C, Rossignol F, Champion E, Combes C, et al. Biomimetic apatite sintered at very low temperature by spark plasma sintering: physico-chemistry and microstructure aspects. Acta Biomater 2010;6:577–85.
[141] Kreidler ER, Hummel FA. Phase relationship in the system $SrO–P_2O_5$ and the influence of water vapor on the formation of $Sr_4P_2O_9$. Inorg Chem 1967;6:884–91.
[142] Monma H, Goto M. Behavior of the alpha<=>beta phase transformation in tricalcium phosphate. Yogyo Kyokai Shi 1983;91:473–5.
[143] Helliott JC. Structure and chemistry of apatites and other calcium orthophosphates. In: Helliott JC, editor. Studies in inorganic chemistry 18. Amsterdam, Elsevier Science BV; 1994.
[144] Akao M, Aoki H, Kato K, Sato A. Dense polycrystalline β-tricalcium phosphate for prosthetic applications. J Mater Sci 1982;17:343–6.
[145] Destainville A, Champion E, Bernache-Assollant D, Laborde E. Synthesis, characterization and thermal behavior of apatitic tricalcium phosphate. Mater Chem Phys 2003;80:269–77.
[146] Descamps M, Hornez JC, Leriche A. Effects of powder stoichiometry on the sintering of β-tricalcium phosphate. J Eur Ceram Soc 2007;27:2401–6.
[147] Zhang F, Lin K, Chang J, Lu J, Ning C. Spark plasma sintering of macroporous calcium phosphate scaffolds from nano crystalline powders. J Eur Ceram Soc 2008;28:539–45.
[148] Douard N, Detsch R, Chotard-Ghodsnia R, Damia C, Deisinger U, Champion E. Processing, physico-chemical characterisation and in vitro evaluation of silicon containing β-tricalcium phosphate ceramics. Mater Sci Eng C 2011;31:531–9.
[149] Itatani K, Nishioka T, Seike S, Howell FS, Kishioka A, Kinoshita M. Sinterability of β-calcium orthophosphate powder prepared by spray-pyrolysis. J Am Ceram Soc 1994;77:801–5.
[150] Tampieri A, Celotti G, Sszontagh F, Landi E. Sintering and characterization of HA and TCP bioceramics with control of their strength and phase purity. J Mater Sci Mater Med 1997;8:29–37.
[151] Famery R, Richard N, Boch P. Preparation of α- and β-tricalcium phosphate ceramics, with and without magnesium addition. Ceram Int 1994;20:327–36.
[152] Jarcho M, Salsbury RL, Thomas MB, Doremus RH. Synthesis and fabrication of β-tricalcium phosphate (whitlockite) ceramics for potential prosthetic applications. J Mater Sci 1979;14:142–50.
[153] Ryu HS, Youn HJ, Hong KS, Chang BS, Lee CK, Chung SS. An improvement in sintering property of β-TCP by addition of calcium pyrophosphate. Biomaterials 2002;23:909–14.
[154] Averbuch-Pouchot MT, Durif A. Topics in phosphate chemistry. Singapore: World Scientific; 1996.
[155] Carbajal L, Caballero A, Sainz MA. Design and processing of ZnO doped tricalcium phosphate based materials: influence of b/a polymorph phase assemblage on microstructural evolution. J Eur Ceram Soc 2012;32:569–77.
[156] Xue W, Dahlquist K, Banerjee A, Bandyopadhay A, Bose S. Synthesis and characterization of tricalcium phosphate with Zn and Mg based dopants. J Mater Sci Mater Med 2008;19:2669–77.
[157] Banerjee SS, Tarafder S, Davies NM, Bandyopadhay A, Bose S. Understanding the influence of MgO and SrO binary doping on the mechanical and biological properties of β-TCP ceramics. Acta Biomater 2010;6:4167–74.
[158] Fielding GA, Bandyopadhay A, Bose S. Effects of silica and zinc oxide doping on mechanical and biological properties of 3-D printed tricalcium phosphate tissue engineering scaffolds. Dental Mater 2012;28:113–22.
[159] Seeley Z, Bandyopadhay A, Bose S. Influence of TiO_2 and Ag_2O addition on tricalcium phosphate ceramics. J Biomed Mater Res 2007;82A:113–21.
[160] Seeley Z, Bandyopadhay A, Bose S. Tricalcium phosphate based resorbable ceramics: influence of NaF and CaO addition. Mater Sci Eng C 2008;28:11–7.
[161] Miranda P, Saiz E, Gryn K, Tomsia AP. Sintering and robocasting of β-tricalcium phosphate scaffolds for orthopaedic applications. Acta Biomater 2006;2:457–66.
[162] Legeros RZ, Lin S, Rohanizadeh R, Mijares D, Legeros JP. Biphasic calcium phosphate bioceramics: preparation, properties and applications. J Mater Sci Mater Med 2003;14:201–9.
[163] Toriyama M, Ravagloili A, Krajewski A, Celotti G, Piancastelli A. Synthesis of hydroxyapatite-based powders by mechano-chemical method and their sintering. J Eur Ceram Soc 1996;16:429–36.
[164] Kivrak N, Tas C. Synthesis of calcium hydroxyapatite–tricalcium phosphate (HA–TCP) composite bioceramic powders and their sintering behavior. J Am Ceram Soc 1998;81:2245–52.
[165] Slosarczyk A, Bialoskorski J. Hardness and fracture toughness of dense calcium-phosphate-based materials. J Mater Sic Mater Med 1998;9:103–8.
[166] Slosarczyk A, Piekarczyk J. Ceramic materials on the basis of hydroxyapatite and tricalcium phosphate. Ceram Int 1999;25:561–5.
[167] Wang X, Fan H, Xiao Y, Zhang X. Fabrication and characterization of porous hydroxyapatite/β-tricalcium phosphate ceramics by microwave sintering. Mater Lett 2006;60:455–8.
[168] Kannan S, Vieira SI, Olhero SM, Torres PMC, Pina S, da Cruz e Silva OAB, et al. Synthesis, mechanical and biological characterization of ionic doped carbonated hydroxyapatite/β-tricalcium phosphate mixtures. Acta Biomter 2011;7:1835–43.
[169] Brown O, McAfee M, Clarke S, Buchanan F. Sintering of biphasic calcium phosphates. J Mater Sci Mater Med 2010;21:2271–9.
[170] Ryu HS, Hong KS, Lee JK, Kim DJ, Lee JH, Chang BS, et al. Magnesia-doped HA/β-TCP ceramics and evaluation of their biocompatibility. Biomaterials 2004;25:393–401.
[171] Raynaud S. Synthèse, frittage et propriétés mécaniques de phosphates de calcium dans le système hydroxyapatite – phosphate tricalcique (Synthesis, sintering and mechanical properties of calcium phosphates in the system HA–TCP). PhD thesis. France: University of Limoges; 1999.
[172] Lukic M, Stojanovic Z, Skapin SD, Macek-Krzmanc M, Mitric M, Markovic S, et al. Dense fine-grained biphasic calcium phosphate (BCP) bioceramics designed by two-step sintering. J Eur Ceram Soc 2011;31:19–27.
[173] Langstaff S, Sayer M, Smith TJN, Pugh SM, Hesp SAM, Thompson WT. Resorbable bioceramics based on stabilized calcium phosphates. Part I: rational design, sample preparation and material characterization. Biomaterials 1999;20:1727–41.
[174] Fellah BH, Layrolle P. Sol-gel synthesis and characterization of macroporous calcium phosphate bioceramics containing microporosity. Acta Biomater 2009;5:735–42.
[175] Li B, Chen X, Guo B, Wang X, Fan H, Zhang X. Fabrication and cellular biocompatibility of porous carbonated biphasic calcium phosphate ceramics with a nanostructure. Acta Biomater 2009;5:134–43.
[176] Rameshbabu N, Prasad Rao K. Microwave synthesis, characterization and in-vitro evaluation of nanostructured biphasic calcium phosphate. Curr Appl Phys 2009;9:529–31.
[177] Daculsi G, Laboux O, Malard O, Weiss P. Current state of the art of biphasic calcium phosphate bioceramics. J Mater Sci Mater Med 2003;14:195–200.
[178] Habibovic P, Yuan H, Van der Valk CM, Meijer G, Van Blitterswijk CA, De Groot K. 3-D microenvironment as essential element for osteoinduction bybiomaterials. Biomaterials 2005;26:3565–75.
[179] Hing KA, Annaz B, Saeed S, Revell PA, Buckland T. Microporosity enhances bioactivity of syntheticbone graft substitutes. J Mater Sci Mater Mad 2005;16:467–75.
[180] Le Nihouannen D, Daculsi G, Saffarzadeh A, Gauthier O, Delplace S, Pilet P, et al. Ectopic bone formation by microporous calcium phosphate ceramicparticles in sheep muscles. Bone 2005;36:1086–93.
[181] Dellinger JG, Wojtowicz AM, Jamison RD. Effects of degradation and porosity on the load bearing properties of model hydroxyapatite bone scaffolds. J Biomed Mater Res 2006;77A:563–71.
[182] Tang F, Fudouzi H, Uchikoshi T, Sakka Y. Preparation of porous materials with controlled pore size and porosity. J Eur Ceram Soc 2004;24:341–4.

[183] Chotard-Ghodsnia R, Lucas S, Pagnoux C, Champion E, Viana M, Chulia D, et al. Elaboration of a well-ordered porous bioceramic via a heterocoagulation colloidal process. Key Eng Mater 2009;396–398:515–8.
[184] Jackson LE, Barrelet JE, Wright AJ. Rietveld analysis in sintering studies of Ca-deficient hydroxyapatite. Key Eng Mater 2004;254–256:297–300.
[185] Nair MB, Babu SS, Varma HK, John A. A triphasic ceramic-coatedporous hydroxyapatite for tissue engineering application. Acta Biomater 2008;4:173–81.
[186] Lu H, Qu Z, Zhou Y. Preparation and mechanical properties of dense polycrystalline hydroxyapatite through freeze-drying. J Mater Sci Mater Med 1998;9:583–7.
[187] Girija EK, Suresh Kumar G, Thamizhavel A, Yokogawa Y, Narayana Kalkura S. Role of material processing on the thermal stability and sinterability of nanocrystalline hydroxyapatite. Powder Tech 2012;2012:190–5.
[188] Ramesh S, Tan CY, Tolouei R, Amiriyan M, Purbolaksono J, Sopyan I, et al. Sintering behavior of hydroxyapatite prepared from different routes. Mater Des 2012;34:148–54.
[189] Raynaud S, Champion E, Berrnache-Assollant D, Tetard D. Dynamic fatigue and degradation in solution of hydroxyapatite ceramics. J Mater Sci Mater Med 1998;9:221–7.
[190] Bohner M. Silicon-susbtituted calcium phosphates – a critical view. Biomaterials 2009;30:6403–6.